Title
Effects of biomass burning, lightning, and convection on O3, CO, and NOy over the tropical Pacific and Australia in August–October 1998 and 1999

Journal
Journal of Geophysical Research, 107(D3)

ISSN
0148-0227

Authors
Kondo, Y
Koike, M
Kita, K
et al.

Publication Date
2003

DOI
10.1029/2001jd000820

Effects of biomass burning, lightning, and convection on O_3, CO, and NO_y over the tropical Pacific and Australia in August–October 1998 and 1999

Y. Kondo,[1] M. Koike,[2] K. Kita,[1] H. Ikeda,[1] N. Takegawa,[1] S. Kawakami,[4] D. Blake,[5] S. C. Liu,[6] M. Ko,[7] Y. Miyazaki,[1] H. Irie,[3] Y. Higashi,[1] B. Liley,[8] N. Nishi,[9] Y. Zhao,[10] and T. Ogawa[4]

Received 10 May 2001; revised 1 November 2001; accepted 20 November 2001; published 11 December 2002.

[1] In situ aircraft measurements of O_3, CO, total reactive nitrogen (NO_y), NO, and non-methane hydrocarbons (NMHCs) were made over the western Pacific Ocean and Australia during the Biomass Burning and Lightning Experiment (BIBLE) A and B conducted in August–October 1998 and 1999. Generally, similar features were seen in the BIBLE A and B data in the latitudinal variations of these species in the troposphere from 35°N to 28°S at longitudes of 120°–150°E. The focus of this paper is to describe the characteristics of air masses sampled at 15°N–10°S (tropical Pacific) and 10°S–28°S (over Australia). With the exception of occasional enhancements in reactive nitrogen seen over New Guinea associated with lightning activities, the tropical Pacific region is distinguished from the rest of the region by smaller concentrations of these trace species. This can be explained in terms of the absence of surface sources over the ocean, lack of stratospheric intrusion, and the preclusion of midlatitude air and air from the west due to active convection throughout the troposphere. The median O_3, CO, NO_y, and NO mixing ratios in tropical air above 4 km were about 15–20 parts per billion by volume (ppbv), 60–75 ppbv, 20–100 parts per trillion by volume (pptv), and 5–40 pptv, respectively. Data obtained from PEM-West A and B conducted in 1991 and 1994 showed similar latitudinal features, although the PEM-West A values were somewhat elevated due to dominating westerly winds in the lower troposphere associated with El Niño. Over Australia, the levels of O_3, CO, NO_y, NO, and NMHCs were elevated throughout the troposphere over those observed in the tropical Pacific both in 1998 and 1999. The effect from biomass burning that occurred in northern Australia was limited to within the boundary layer because of strong subsidence in the period. Analyses based on 14-day back trajectories identified free tropospheric air over Australia that originated from Indonesia, the Indian Ocean, Africa, and southern midlatitudes. The levels of O_3, CO, NO_y, and NMHCs in these air masses were much higher than those from the tropical Pacific due to their stronger sources from biomass burning and lightning. These values are compared with those obtained in the South Pacific during PEM-Tropics A. Effects of biomass burning and lightning are discussed as possible sources of O_3 and its precursors in these air masses. *INDEX TERMS:* 0368 Atmospheric Composition and Structure: Troposphere—constituent transport and chemistry; 0322 Atmospheric Composition and Structure: Constituent sources and sinks; 0345 Atmospheric Composition and Structure: Pollution—urban and regional (0305); *KEYWORDS:* BIBLE, biomass burning, lightning, ozone, NO_y, tropics

Citation: Kondo, Y., et al., Effects of biomass burning, lightning, and convection on O_3, CO, and NO_y over the tropical Pacific and Australia in August–October 1998 and 1999, *J. Geophys. Res.*, *107*, 8402, doi:10.1029/2001JD000820, 2002. [printed *108*(D3), 2003]

[1]Research Center for Advanced Science and Technology, University of Tokyo, Tokyo, Japan.
[2]Department of Earth and Planetary Sciences, University of Tokyo, Tokyo, Japan.
[3]Solar-Terrestrial Environment Laboratory, Nagoya University, Toyokawa, Japan.
[4]National Space Development Agency of Japan, Earth Observation Research Center, Tokyo, Japan.
[5]Department of Chemistry, University of California, Irvine, California, USA.
[6]Institute of Earth Sciences, Academia Sinica, Taipei, Taiwan, Republic of China.
[7]Atmospheric and Environmental Research Inc., Lexington, Massachusetts, USA.
[8]National Institute of Water & Atmospheric Research, Lauder, New Zealand.
[9]Department of Earth and Planetary Science, Kyoto University, Kyoto, Japan.
[10]Department of Mechanical and Aeronautical Engineering, University of California Davis, California, USA.

0148-0227/02/2001JD000820

1. Introduction

[2] Ozone is produced by chemical reactions initiated by oxidation of CO, CH_4, and non-methane hydrocarbons (NMHCs) by OH in the troposphere. NO acts as an important catalyst in these reactions. The rate of ozone production is predicted to increase almost linearly with NO mixing ratios up to a few thousands of parts per trillion (pptv) in the boundary layer and a few hundreds of pptv in the upper troposphere [*Klonecki and Levy*, 1997]. The O_3 production rate is often limited by the amount of available NO_x (NO and NO_2) in remote regions distant from anthropogenic sources.

[3] In many regions, including over the Pacific, O_3 and its precursors exhibit large latitudinal variations due mainly to the strong latitudinal dependence of their sources and sinks, as well as inputs from the stratosphere [*Kondo et al.*, 1993; *Kawakami et al.*, 1997; *Singh et al.*, 1998; *Emmons et al.*, 1997, 2000]. Emission of NO_x is at a maximum at northern midlatitudes [*Levy et al.*, 1999], reflecting fossil fuel usage. In addition, influxes of O_3 and NO_y from the stratosphere are much larger at midlatitudes than at tropical latitudes. These factors led to positive latitudinal gradients of O_3 and NO_y from the equator to northern midlatitudes over the western Pacific as observed during the aircraft missions Pacific Exploratory Mission-West (PEM-W)-A and B [*Kawakami et al.*, 1997]. Lightning activity is most intense in the tropics and production of NO_x by lightning can be important in maintaining the levels of reactive nitrogen over the tropical Pacific Ocean, which is relatively free from anthropogenic sources. In the southern midlatitudes, NO_x emissions from fossil fuel combustion are much smaller than in northern midlatitudes, increasing the relative importance of the contribution from emissions by biomass burning and lightning [*Levy et al.*, 1999]. Over the South Pacific, biomass burning greatly enhanced O_3 and its precursors in August–September 1996 during the Pacific Exploratory Mission-Tropics (PEM-T)-A [*Gregory et al.*, 1999: *Fenn et al.*, 1999; *Blake et al.*, 1999].

[4] Distributions of various trace gases from the northern to southern midlatitudes over the western Pacific Ocean were measured during the Biomass Burning and Lightning Experiment (BIBLE) A and B aircraft campaigns conducted by the National Space Development Agency of Japan (NASDA) in September–October 1998 and August–September 1999. The Gulfstream-II (G-II) aircraft was used as the primary sampling platform. The major objectives of the BIBLE missions were to investigate the effects of biomass burning and lightning on the distributions of O_3 and its precursor gases as well as aerosols over tropical Indonesia and northern Australia. Detailed descriptions of the meteorological conditions during the BIBLE missions are given by *Nishi* [2001]. These data sets extended measurements of the latitudinal variations of the trace gases obtained during PEM-W-A and B to the Southern Hemisphere. They also enabled comparison with measurements over the South Pacific during PEM-T-A. In this paper, distributions of O_3, NO_y, NO, CO, and some NMHCs over the western and tropical Pacific Ocean and Australia are presented.

2. Aircraft Data

[5] BIBLE A and B were conducted during 24 September to 10 October 1998 and 30 August to 14 September 1999, respectively. The flight tracks of the aircraft measurements are shown in Figure 1. More detailed flight tracks are also available at (http://www.eorc.nasda.go.jp/AtmChem/GLACE/bible/BIBLE.html). Values of O_3, NO_y, NO, CO, C_2H_6, C_3H_8, n-C_4H_{10}, CH_3Cl, and C_2Cl_4 observed along the flight tracks are used for this paper. Ozone was measured by a UV photometer [*Kita et al.*, 2002], and NO and NO_y were measured with a chemiluminescence technique combined with a gold catalytic converter [*Kondo et al.*, 1997a; *Koike et al.*, 2000]. These three gases were measured with 1-second (s) time resolution. Carbon monoxide was measured by a gas chromatographic technique during BIBLE A and B with 20-s resolution [*Kita et al.*, 2002] and by a VUV resonance fluorescence technique with 1-s resolution during BIBLE B [*Takegawa et al.*, 2001]. Both CO measurement techniques agreed to within 6%. Because of the faster response of the resonance fluorescence measurements, they were used for the analysis of BIBLE B data. The O_3, NO_y, NO, and CO values were averaged for 10 or 60 s. The NMHC measurements were made by whole air sampling [*Blake et al.*, 1996] with 5-min resolution on average.

[6] The measurements obtained in the longitude range between 120°E and 150°E (Figure 1) are used as the primary source of data for this analysis. The observations over Indonesia during BIBLE A have been discussed by *Kita et al.* [2002] and *Koike et al.* [2002]. Altitude profiles of the trace species were obtained during takeoff and landing in Nagoya (36°N), Saipan (15°N), Biak (1°S), Port Moresby (10°S), Darwin (12°S), Cairns (16°S), and Alice Springs (23°S). These data, together with those obtained during constant-altitude flight legs, are used in this paper.

3. Latitudinal Variations

3.1. Upper Troposphere

[7] Observed features of O_3, CO, NO_y, NO, C_2H_6, and C_3H_8 are described first for the purpose of classifying air masses based on their distinctive latitudinal variations. Mixing ratios of these species observed above 8 km during BIBLE A and B are plotted versus latitude in Figure 2. The back trajectories were calculated using the method developed by *Matsuzono et al.* [1998] and the European Centre for Medium-Range Weather Forecasts (ECMWF) data on a 2.5° × 2.5° latitude-longitude grid. For example, Figure 3 shows 10-day kinematic back trajectories of air masses sampled above 8 km during the BIBLE A southbound flights.

[8] The levels of O_3, CO, and NO_y at 15°–34°N were highly variable, with ranges of 20–80 parts per billion by volume (ppbv), 70–250 ppbv, and 30–1200 pptv, respectively, reflecting varying influences from different sources. North of 15°N, the air masses were generally transported from higher latitudes along clockwise flow due to the high pressure system persistent over the northeastern Pacific in this season, as was observed during PEM-W-A [*Gregory et al.*, 1996, 1997]. At 15°–23°N, the air masses remained over the ocean longer than those at higher latitudes (Figure 3). The O_3, CO, and NO_y values often showed abrupt changes at latitudes between 15° and 23°N, corresponding to the changes in the air mass origin at mid- or subtropical latitudes as determined by trajectories.

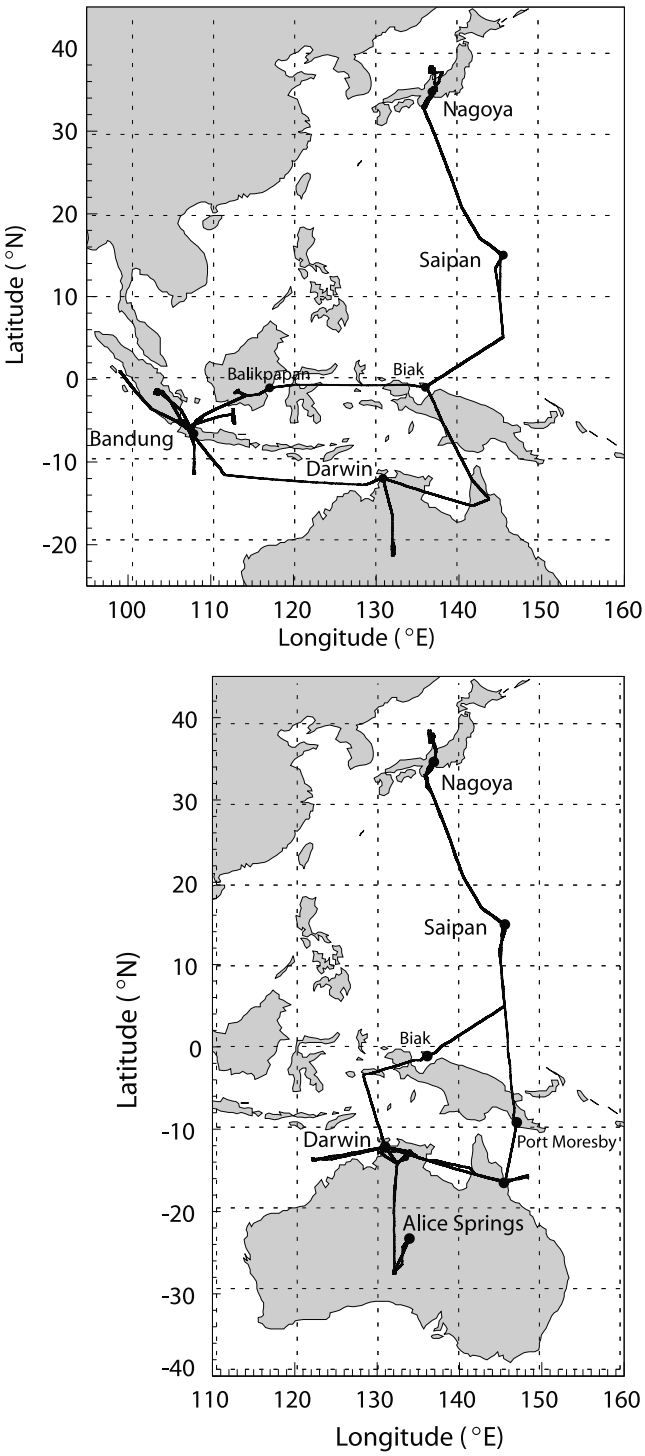

Figure 1. Flight routes for BIBLE (top) A and (bottom) B.

[9] At 15°N–10°S, the levels of O_3, CO, NO_y, and NO were much lower and less variable than at 15°–34°N. The air masses remained over the tropical Pacific Ocean for at least several days. South of 10°S, the levels and variabilities of these species showed abrupt increases. Namely, the ranges of O_3, CO, and NO_y increased to 15–120 ppbv, 60–140 ppbv, and 100–1000 pptv, respectively, as shown in Figure 2. Some of the air masses with enhanced concentrations of O_3, CO, and NO_y had passed over Africa, South America, or Indonesia.

3.2. Altitude-Meridional Distribution

[10] Figures 4a and 4b show meridional distributions of O_3, CO, NO_y, and NO along the longitudes of 120°–150°E constructed using altitude profiles obtained near Saipan, Biak, Port Moresby, Darwin, Cairns, and Alice Springs, in addition to the constant-altitude leg data shown above. These meridional cross sections are smoothed contours of the data averaged for 1° in latitude and 1 km in altitude. Three distinct regimes of air for different latitude ranges are clearly defined as "northern midlatitude" north of 15°N, "tropical Pacific" for the zone of 15°N–10°S, and "southern hemisphere" south of 10°S, although the locations of the boundaries varied between 1998 and 1999 and depended on altitude to some extent. It should be noted that small-scale variability appearing in the contours may not be representative of the real vertical variability because the contours were produced by interpolating the grid points vertically and horizontally. For example, the vertical extent of the enhanced NO_y and NO values centered at 10.5 km near 20°N seen in Figures 4a and 4b was determined simply by interpolating the enhanced values at this altitude level (shown in Figure 2) and the other data at different altitudes, which were obtained on a different day. Because of their interesting characteristics, we hereafter focus on the analysis of the tropical Pacific Ocean and the Southern Hemispheric air masses. Table 1 summarizes the CO, O_3, NO_y, and NO median values obtained in the tropical Pacific air during BIBLE A and B, PEM-W-A [*Kondo et al.*, 1996], PEM-W-B [*Kawakami et al.*, 1997], and PEM-T-A [*Gregory et al.*, 1999], together with the phases of El Niño-Southern Oscillation (ENSO).

4. Tropical Pacific Ocean

4.1. Effect of Convection

[11] Deep convective activity can be identified by the relatively high probability of existence of optically thick clouds above 8 km, as described by *Kita et al.* [2002]. Figure 5 shows the average probability distribution during BIBLE A and B, estimated using Geostationary Meteorological Satellite (GMS)-5 infrared cloud image data. The tropical Pacific region bounded by 15°N–10°S and 120°–150°E was covered with convective clouds 30–60% of the time during BIBLE A and 30–50% for BIBLE B. In addition, the region of high rainfall rate in September over the tropical Pacific Ocean observed by the Precipitation Radar (PR) and Tropical Rainfall Measuring Mission (TRMM) Microwave Imager (TMI) on board the TRMM satellite (http://www.eorc.nasda.go.jp/TRMM/imgdt/L3_data/index.htm) coincides with the region of persistent high clouds (not shown). This is the region where the Intertropical Convergence Zone (ITCZ) and South Pacific Convergence Zone (SPCZ) merged. La Niña prevailed in 1998 but it weakened significantly by September 1999. Higher convective activity in 1998 than in 1999 corresponds to the higher sea surface temperature (SST) associated with La Niña.

[12] The origin of the tropical air can be identified by back trajectories and streamlines. Typically, as shown in Figure 3, upper tropospheric air was transported from the lower troposphere or boundary layer within 10 days through the extensive convection in the ITCZ. A detailed analysis of

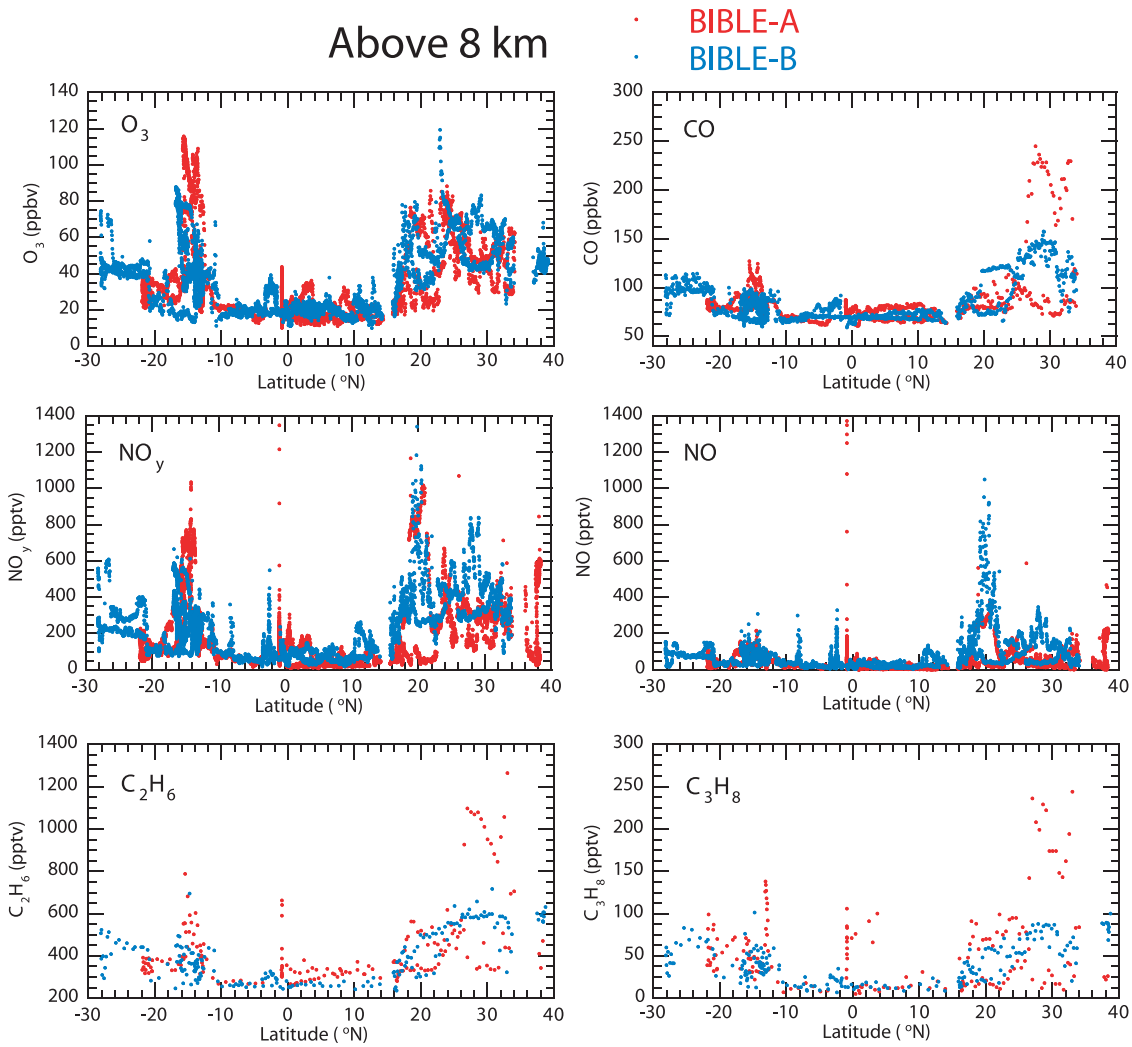

Figure 2. Latitudinal variations of O_3, CO, NO_y, NO, C_2H_6, and C_3H_8 above 8 km during BIBLE A (red) and B (blue).

all 10-day back trajectories for upper tropospheric air masses sampled at 15°N–10°S during BIBLE A and B showed that they remained in the same latitude range for 10 days prior to sampling and originated from the boundary layer or lower troposphere in the zone of 130°–180°E, as seen in Figure 3. The vertical velocities calculated by ECMWF are the average values near the ITCZ, thus the cluster of trajectories, if they reasonably converge, as is the case for the present study, should be considered to represent the mean motion of the tropical air masses. The vertical transport of an air mass within a convective cloud occurs much faster than that represented by the trajectory. In addition, mid-tropospheric air can be entrained during upward transport from the boundary layer. To supplement the trajectory analysis in identifying the origin of the tropical air, the average streamlines at 200, 500, and 850 hPa during BIBLE B are shown in Figure 6. The average streamlines during BIBLE A are similar to those during BIBLE B. They indicate that the air between the boundary layer and mid-troposphere in the zone of 130°–180°E was generally transported from the east before upward transport in the ITCZ. The trajectories and streamlines demonstrate

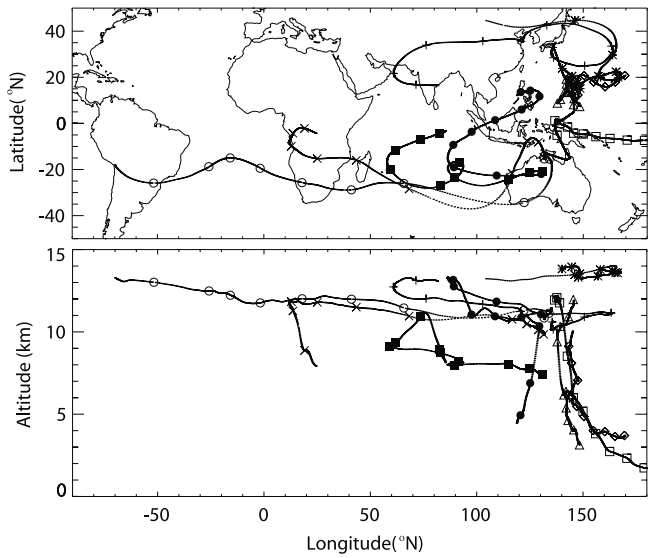

Figure 3. Ten-day back trajectories for air masses sampled during the southbound flights of BIBLE A.

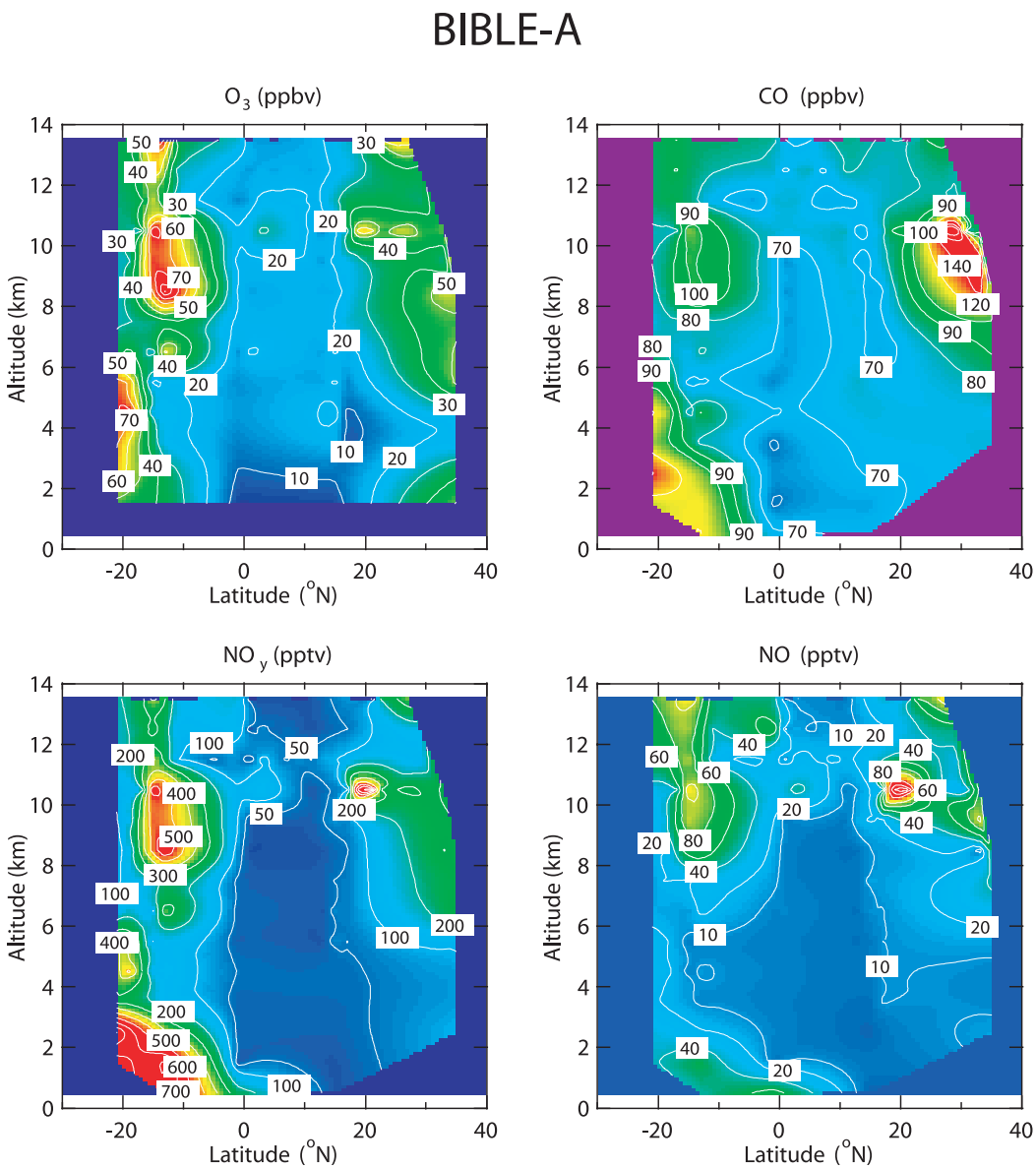

Figure 4a. Meridional cross sections of O_3, CO, NO_y, and NO constructed from the data obtained during BIBLE A.

that the tropical Pacific air was nearly completely isolated from midlatitude air.

[13] Figure 7 shows the altitude profiles of the O_3, CO, NO_y, and NO mixing ratios obtained between Saipan and Biak (15°N–5°S, east of 135°E) over the tropical Pacific Ocean. The ranges of their median mixing ratios at different altitudes were 5–20 ppbv, 60–75 ppbv, 20–100 pptv, and 5–40 pptv, respectively. The median O_3, CO, NO_y, and NO mixing ratios at 0.5–4 km were in the ranges of 5–15 ppbv, 60–75 ppbv, 20–70 pptv, and 3–5 pptv, respectively, indicating that the influence of anthropogenic emissions of O_3 precursors on the abundances of O_3 and reactive nitrogen was small in the boundary layer over the tropical Pacific.

[14] The effect of O_3 production has also been investigated by calculating the photochemical production (P), loss (L), and net production (P–L) terms calculated with a box model [*Ko et al.*, 2002], using the observed NO, O_3, H_2O, and J_{O_3} values. For the region of study, P and L terms are approximated as

$$P = \{k_{NO+HO_2}[HO_2] + k_{CH_3O_2+NO}[CH_3O_2]\}[NO] \quad (1)$$

$$L = \{k_{H_2O+O(^1D)}J_{O_3}f[H_2O] + k_{OH+O_3}[OH] + k_{HO_2+O_3}[HO_2]\}[O_3] \quad (2)$$

where [ ] denotes the concentration of the assigned species, k_{X+Y} is the reaction rate coefficient for the reaction X + Y → products, J_{O_3} is the photolysis rate coefficient of O_3, and f is defined so that J_{O_3} f[O_3] is [$O(^1D)$]. The model calculations indicate that the net O_3 production rate was close to zero at observed low concentrations of NO and O_3.

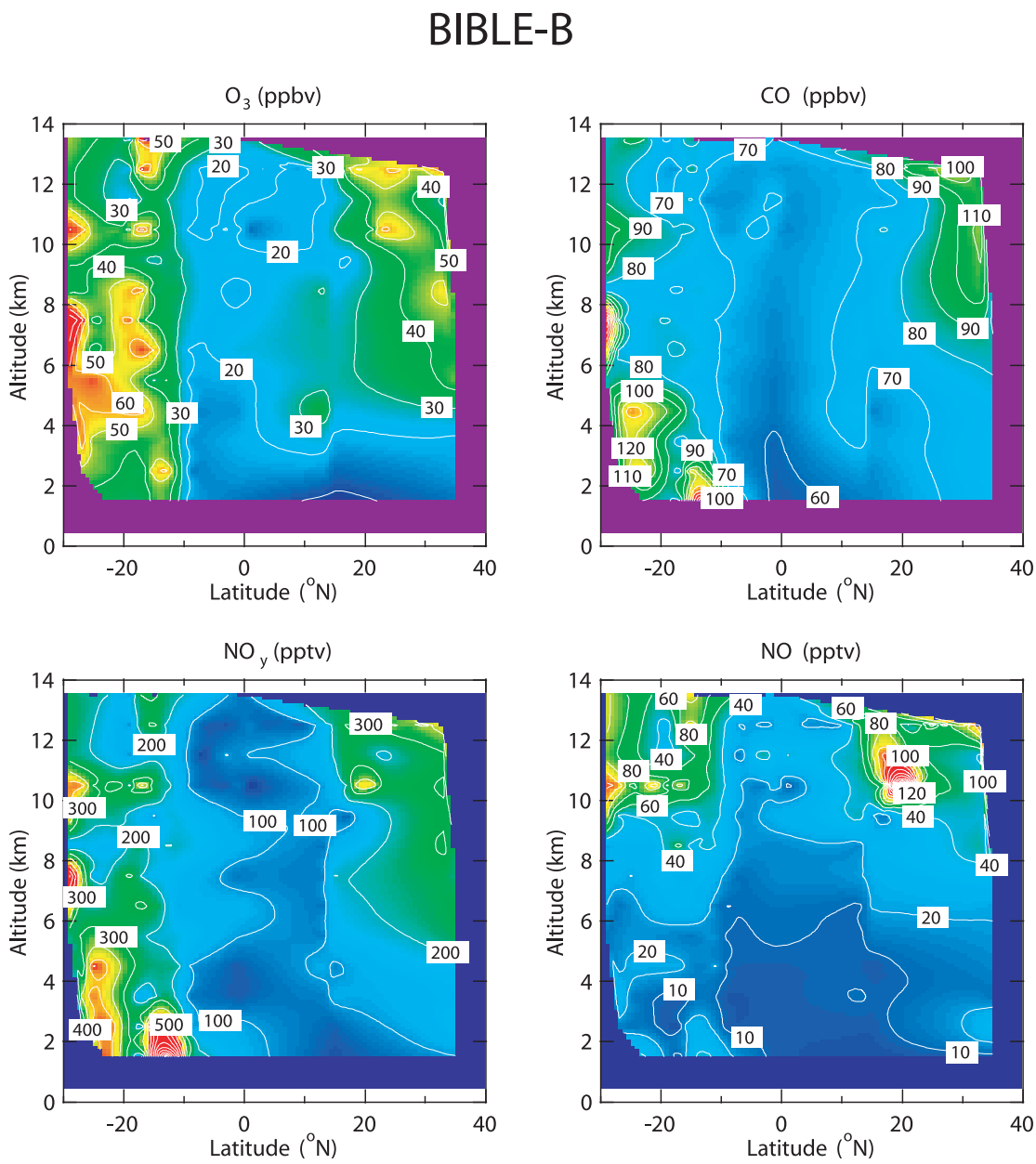

Figure 4b. Same as Figure 4a but for BIBLE B.

Transport of boundary layer and lower tropospheric air poor in O_3, NO_y, and NO to the upper troposphere should strongly control the level of these species throughout the troposphere.

[15] The dominant component of NO_y in the maritime boundary layer was HNO_3 during PEM-W-B [*Kondo et al.*, 1997b], presumably due to rapid oxidation of NO_x by OH. HNO_3 is removed by deposition and also dissolves in cloud

Table 1. Median Values of O_3, CO, NO, and NO_y Obtained above 8 km Over the Tropical Pacific and South Pacific Ocean[a]

	Mission				
	BIBLE A	BIBLE B	PEM-W-A	PEM-W-B[b]	PEM-T-A
ENSO	La Niña	La Niña	El Niño	El Niño	Neutral/weak La Niña
O_3 (ppbv)	19 (16)	20 (18)	26 (26)	19 (18)	35 (34)
CO (ppbv)	72 (67)	67 (66)	101 (96)	86 (83)	59 (54)
NO_y (pptv)	62 (32)	70 (75)	145 (142)	53 (104)	131 (115)
NO (pptv)	18 (5)	24 (10)	19 (8)	8 (6)	27 (8)

[a]The numbers in the brackets are the values at 4–8 km. BIBLE A and B values are for 120–150°E and 15°N–10°S. PEM-W-A and B values are for the same longitudes but at 15°N–0°N. PEM-T-A data are for the South Pacific bounded by SPCZ and ITCZ [*Gregory et al.*, 1999].

[b]Data strongly influenced by emissions from South East Asian continent [*Kawakami et al.*, 1997] were excluded.

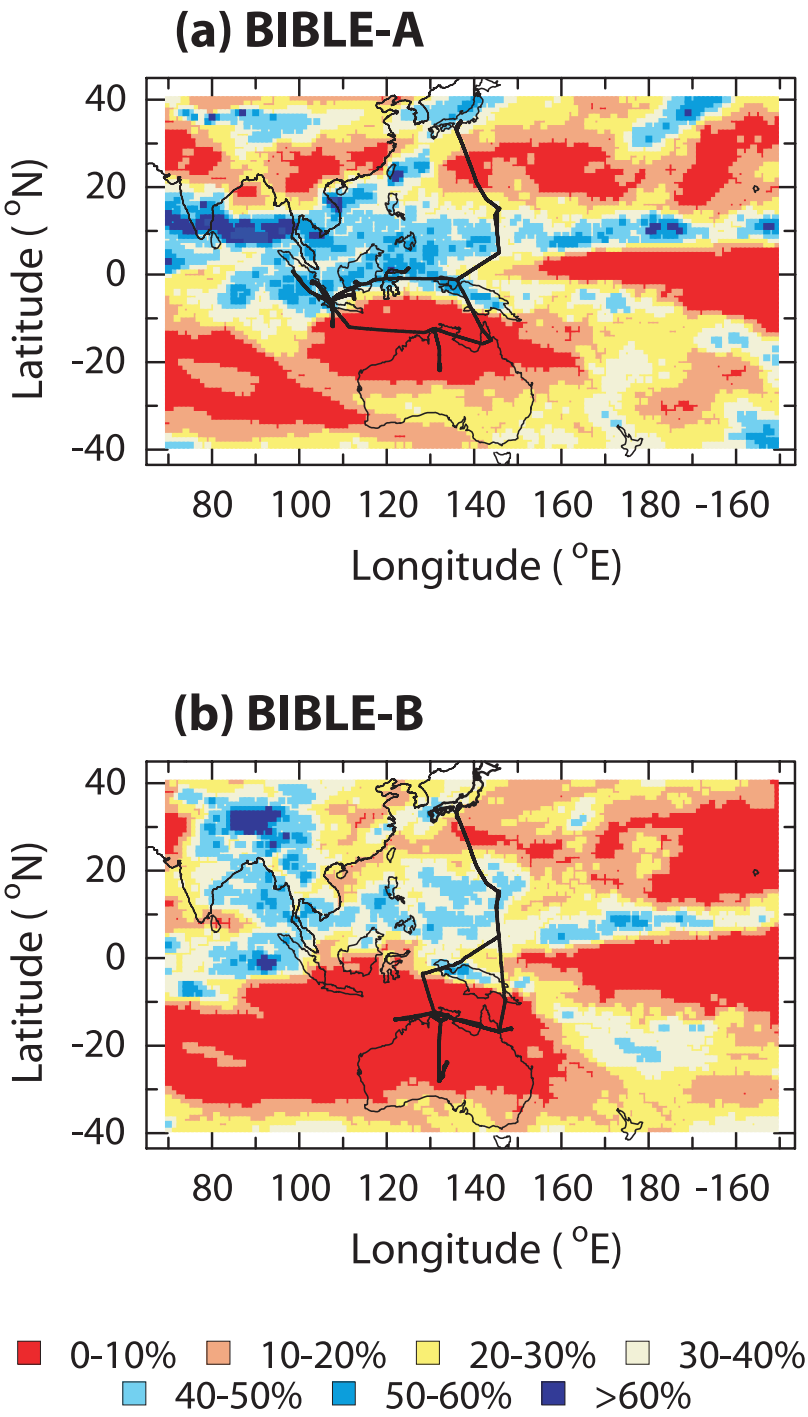

Figure 5. Probability of convective cloud cover during BIBLE A and B.

droplets, which are removed by precipitation. High precipitation rates in the tropical Pacific, as observed by TRMM, should effectively remove NO_y.

4.2. Effect of Lightning

[16] There were cases when the NO and NO_y values showed enhancements above the low background values of the tropical Pacific. During flight 13 of BIBLE A, made on 9 October 1998, the NO and NO_y mixing ratios at 13 km showed a sharp peak reaching 1400 pptv when the G-II flew close to the anvil of a cumulous cloud at 1°S and 131°E over northwestern New Guinea, as seen in Figure 2. During this encounter, the NO/NO_y ratio was close to 1. The data shown in Figure 7 do not include the 1400 pptv NO data. During flight 11 of BIBLE B, made on 12 September 1999, the NO and NO_y values at 13 km occasionally reached 100–300 pptv and 300–500 pptv, respectively, at 2°–10°S between Darwin and Biak, without significant changes in CO, as seen in Figures 2 and 7.

[17] Statistically, lightning activity was high over New Guinea in October 1998 and September 1999 as observed by the Optical Transient Detector (OTD) on board the

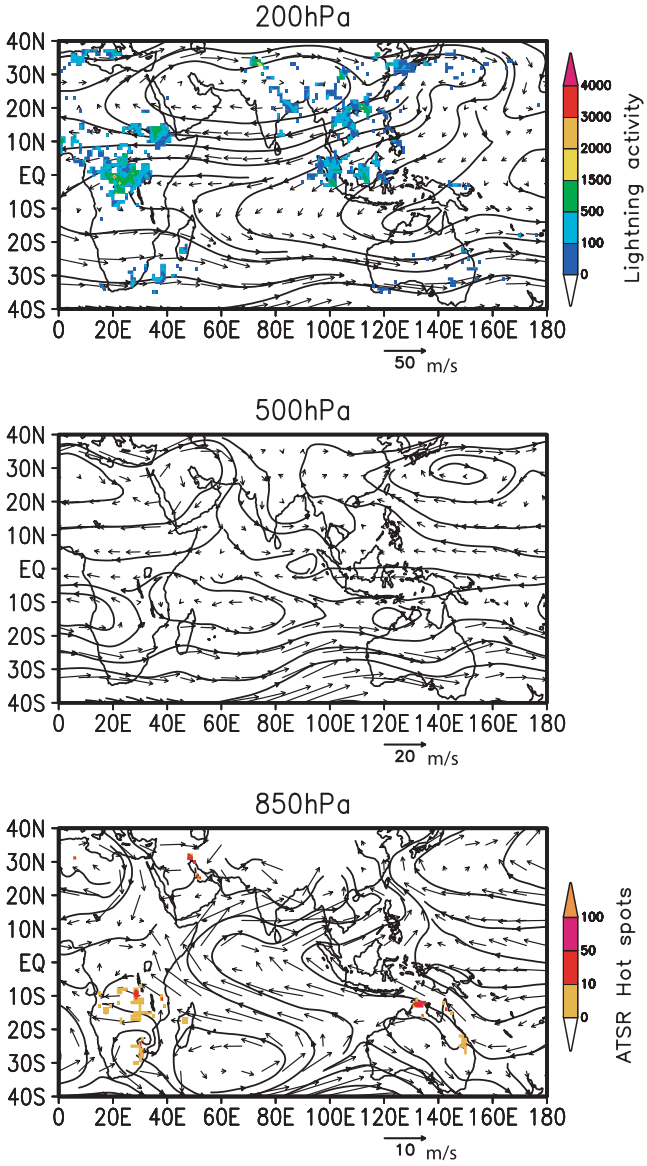

Figure 6. Average streamlines and wind vectors at 200, 500, and 850 hPa during BIBLE B. The streamlines at 200 and 850 hPa are overlaid with the LIS lightning and ATSR hot spot data for BIBLE B, respectively.

MicroLab satellite (http://thundr.msfc.nasa.gov/otd/) [*Nesbitt et al.*, 2000] and Lightning Imaging Sensor (LIS) on board TRMM (http://thundr.msfc.nasa.gov/lis/). The probability of convective activity over New Guinea was also high (>50%) during BIBLE A and B, as seen from Figure 5, consistent with the OTD and LIS data. It is very likely that these high NO values were due to NO production by lightning near New Guinea. Similar enhancements in NO and NO_y reaching 900 pptv were observed at 9.5 km at 4–6°S near the coast of New Guinea in February 1994 during PEM-W-B [*Kawakami et al.*, 1997]. Enhancements in NO were observed three times out of six flights in this region during BIBLE A and B and PEM-W-B, suggesting that high NO frequently occurs near New Guinea, especially during October–March. Lightning over the tropical islands may play a role in maintaining the levels of reactive nitrogen in the upper troposphere over the tropical Pacific, as seen in Figure 7.

[18] The median O_3 values at 9–12 km shown in Figure 7 were higher by about 5 ppbv than those at 8 and 13 km, coinciding with the increases in NO_y and NO. All the O_3 values obtained between Saipan and Biak above 8 km during BIBLE A and B are plotted against the NO_y and NO values in Figure 8, except for the flight 11 data of BIBLE A that was influenced by very recent lightning. O_3 was well correlated with NO_y and NO in moderately aged air masses with NO/NO_y ratios lower than 0.45. The O_3 values increased from about 15 ppbv to 35 ppbv with increases in NO_y (NO) from 25 (5) pptv to 150 (50) pptv. Even in air masses relatively fresh in NO ($NO/NO_y > 0.45$), O_3 was correlated with NO_y and NO. The O_3 values in these air masses were 10–15 ppbv lower than those in aged air ($NO/NO_y < 0.45$).

[19] The net ozone production rates (P–L) in the tropical air above 4 km calculated with the box model are shown versus the measured NO values in Figure 9. At an NO mixing ratio of 50 pptv, the net ozone production rate is 1–1.3 ppbv/d. Immediately after NO production by lightning, the NO values should be close to the NO_y values. NO_y values corresponding to 50 pptv NO were about 150–200 pptv (Figure 8). At NO values of 150–200 pptv, the net production will exceed 2 ppbv/d. Ozone should increase by 10 ppbv within 3–5 days in these air masses. It is difficult to estimate the residence time of the air masses after NO production by lightning because of uncertainties in the trajectories influenced by convection, as discussed in section 4.1.

4.3. Comparison With PEM-W and PEM-T-A Data

[20] The median values of O_3, CO, and NO_y in the tropical region during PEM-W-A were somewhat higher than those during BIBLE A and B, although they were obtained in the same season (September–October), as shown in Table 1. The PEM-W data are for the latitudes of 15°N–0°N. During PEM-W-A (El Niño), the location of intensive convection over the western Pacific shifted to the east as compared with that during La Niña, as seen from the GMS-5 data (not shown). Associated with this, westerly winds prevailed in the boundary layer and lower troposphere over the western Pacific, transporting air impacted by Southeast Asia to the tropical Pacific at 120°E–150°E, as shown in Figure 10. Intensive convection in this region transported this moderately polluted air to the upper troposphere. By contrast, tropical Pacific air in the lower troposphere was transported from the central Pacific Ocean during BIBLE A (Figure 10) and BIBLE B (Figure 6), as is typical for La Niña periods.

[21] During PEM-W-B (February–March 1994), the lower troposphere in the tropical Pacific Ocean was dominated by easterlies (Figure 10), as is typical for this season, irrespective of the ENSO phase. The similarity in the O_3, CO, and NO_y values in the tropical free troposphere during PEM-W-B to those during BIBLE A and B can be interpreted as due to the similarity in the origins of the air, namely boundary layer/lower troposphere over the central Pacific Ocean.

[22] Table 1 also summarizes the PEM-T-A data sampled over the Central Pacific at 10°N–20°S and 170°E–140°W

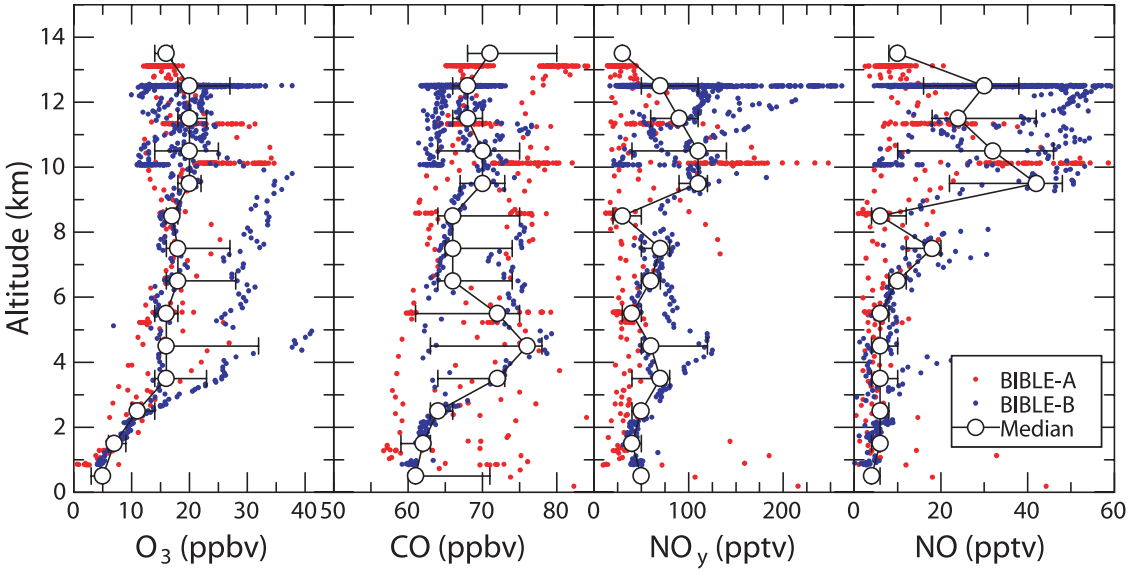

Figure 7. Altitude profiles of O_3, CO, NO_y, and NO obtained at latitudes between Saipan and Biak during BIBLE A (red points) and B (blue). Median values with 1-km intervals are also shown (open circles). The bars represent the central 50% of the range.

[*Gregory et al.*, 1999]. The O_3 and NO_y mixing ratios during BIBLE A and B were considerably lower than those during PEM-T-A, although the CO values were higher. Center of the large-scale convective activity was located over the western Pacific (Figure 5), much closer to the region of the BIBLE measurements than that of PEM-T-A [*Fuelberg et al.*, 1999]. The higher convective activity over the western Pacific leads to lower O_3 and NO_y levels, as discussed in section 4.1. CO has a much longer lifetime and is controlled by sources and sinks at a much larger regional scale.

5. Southern Hemispheric Air

[23] During BIBLE B, biomass burning activity was high over northern Australia, as seen in the Advanced Very High Resolution Radiometer (AVHRR) and Along Track Scanning Radiometer (ATSR) World Fire Atlas data (http://shark1.esrin.esa.it/FIRE/AF/ATSR/) [*Russell-Smith et al.*, 2002]. Fresh biomass burning plumes were sampled near Darwin by the G-II during flights 6 and 7, conducted on 2 and 4 September 1999, as discussed by *Shirai et al.* [2002]. Strong enhancements of NO_y, CO, and C_2H_6 reaching as high as 15 ppbv, 1000 ppbv, and a few ppbv, respectively, were observed in these plumes encountered below 3 km. The mixing ratios of these species sharply decreased with altitude above about 3 km, which is the approximate top of the boundary layer. It was found that biomass burning plumes in northern Australia during BIBLE B were mostly confined to the boundary layer due to strongly subsiding air associated with the high pressure system located northwest of Australia [*Nishi*, 2001]. The region of subsidence coincides with the region of very low cloud cover in northern Australia, as seen in Figure 5.

[24] During the BIBLE A period, biomass burning activities in northern Australia sighted on board the G-II seemed to be considerably lower than those sighted during BIBLE B. However, some biomass burning activity during the BIBLE A period can be seen from the ATSR data. The effect of biomass burning in northern Australia is reflected in the enhancement of the CO and NO_y levels below 3 km at 10°–20°S, as seen in Figures 4a and 4b.

[25] In the free troposphere above 4 km, enhanced values of O_3, CO, NO_y, and NO were often observed south of 10°S during BIBLE A and B. These enhancements were often associated with those in NMHCs such as C_2H_6 and C_3H_8 (Figure 2). These air masses did not originate from the boundary layer of northern Australia but were transported from regions outside Australia. In the following section, we focus on the chemical characteristics of the free tropospheric air observed over Australia.

5.1. Air Mass Categories and Median Values

[26] Air masses observed at 10°–30°S over Australia above 4 km were classified using 14-day back trajectories. Typical trajectories of air masses sampled above 8 km during BIBLE A are shown in Figure 3. The average streamlines and wind vectors at 200, 500, and 850 hPa during BIBLE B shown in Figure 6 are also useful in identifying the origins of air masses. The streamlines at 200 and 850 hPa are overlaid with the LIS lightning and ATSR hot spot data for BIBLE B, respectively. Air masses transported from over Indonesia are defined as Indonesian air. Many of them were carried upwards from the lower troposphere by strong convection over the Indonesian region as shown in more detailed trajectories for BIBLE B (Figure 11a). Some air masses were transported from over the Indian Ocean, passing over the African continent east of 20°E (Indian Ocean A) or without passing over the African continent (Indian Ocean B), as shown in Figures 11b and 11c (BIBLE B) and Figure 2 (BIBLE A). The Indian Ocean A and B air underwent strong uplift over the Indian Ocean due to convective activity in this region. The eastern part of the convective region over the Indian Ocean is seen in

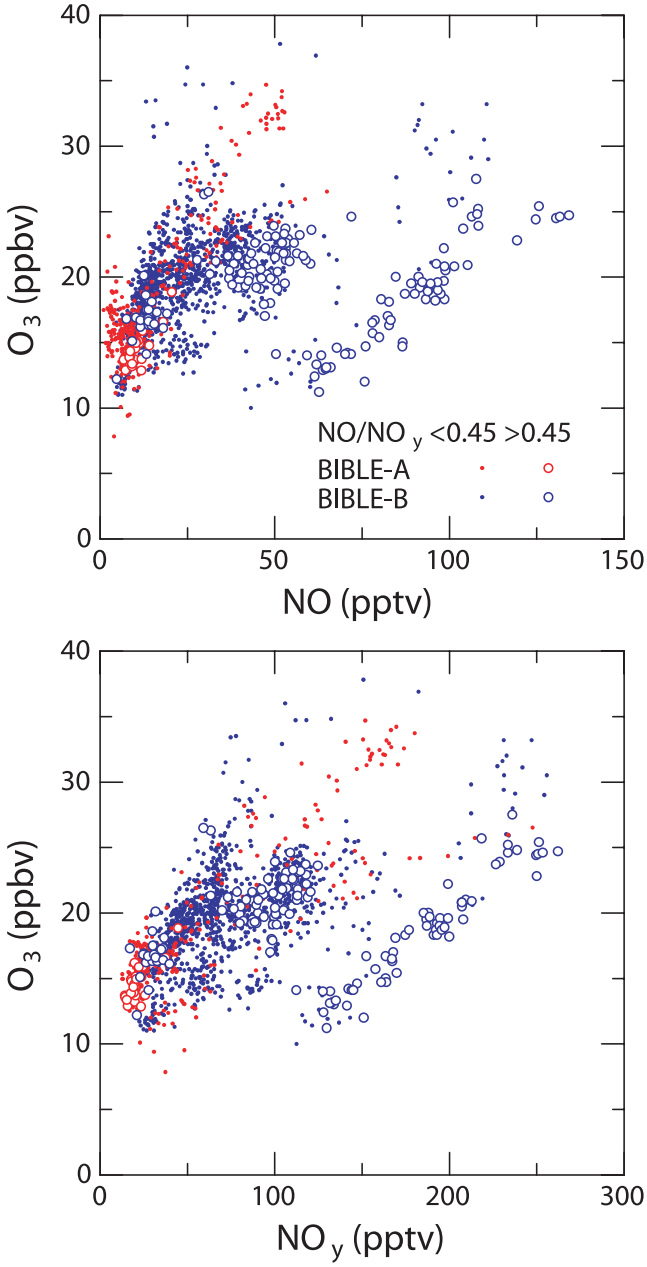

Figure 8. O_3-NO and O_3-NO_y correlations in air masses sampled above 8 km between Saipan and Biak (15°N–5°S, east of 135°E) during BIBLE A (red) and B (blue). Solid and open circles are for NO/NO_y ratios lower and higher than 0.45, respectively.

Figure 5 and also in NCEP Outgoing Long-wave Radiation (OLR) maps (http://wesley.wwb.noaa.gov/ncep_data/) for the entire Indian Ocean. Hence, the Indian Ocean A and B air sampled in the upper or middle troposphere originated from the lower troposphere or boundary layer over the Indian Ocean. Air masses originating from central Africa or the tropical Atlantic Ocean at 25°W-20°E are defined as African air (Figure 3). These air masses were carried upward to some extent near tropical Africa or the Atlantic Ocean due to persistent convective activity in this region. Air masses that reached South America are defined as south midlatitude, because they rarely reached regions with latitudes lower than 10°S (Figure 3). They stayed mainly between 20°–40°S for 14 days or longer prior to sampling. Their trajectories for air masses above 8 km are shown in Figure 12, together with those for African air masses. The trajectories are overlaid with the LIS lightning and ATSR hot spot data for BIBLE A and B. The trajectories for south midlatitude air did not show large altitude changes. Some of the south midlatitude air masses in the upper troposphere were carried around the earth in 12 days.

[27] Table 2 summarizes the median values of the 10-s averaged O_3, CO, NO_y, and NO data and more sparsely collected C_2H_6, C_3H_8, and CH_3Cl data for each of the different air masses discussed above. The data observed over Indonesia during BIBLE A are also given for comparison. Biomass burning activity in this region during BIBLE A was lower than average and is discussed in detail by *Kita et al.* [2002]. The median values of these species in the upper troposphere in each air mass are also shown in Figures 13a and 13b In addition, the median C_3H_8/C_2H_6 and n-C_4H_{10}/C_2H_6 ratios are also shown for comparison. The slopes of the C_3H_8-C_2H_6 correlation ($\Delta C_3H_8/\Delta C_2H_6$) were also derived (not shown), although the C_3H_8-C_2H_6 correlation was generally poor except for the Indonesian air. The C_3H_8/C_2H_6 ratios and $\Delta C_3H_8/\Delta C_2H_6$ values were similar except for the south midlatitude air, in which the $\Delta C_3H_8/\Delta C_2H_6$ value was much lower than the C_3H_8/C_2H_6 ratio. Meaningful slopes for the n-C_4H_{10}-C_2H_6 correlation were not obtained due to very poor correlations. The lifetimes of C_2H_6 and C_3H_8 at 0–4 km are about 20 and 4 days, respectively, and 100 and 16 days at 8–12 km [*Mauzerall et al.*, 1998]. The lifetime of n-C_4H_{10} is a few days in the upper troposphere. The C_3H_8/C_2H_6 and n-C_4H_{10}/C_2H_6 ratios are qualitative indicators of air mass age, though mixing processes also alter the hydrocarbon ratios [*McKeen and Liu*, 1993; *McKeen et al.*, 1996].

[28] The median values for the tropical Pacific air are shown in Figures 13a and 13b for comparison. The Indian Ocean B data during BIBLE A are not shown due to their paucity. Indian Ocean A air masses during BIBLE A passed over Africa where convection was active, and their median values were similar to the African air. These data were also excluded from Figures 13a and 13b because of possible influence from the African continent.

[29] It should be noted that there are some limitations in characterizing the chemical compositions of these air masses using this method. First, identification of the air mass origins can sometimes be largely uncertain due to errors in the 14-day back trajectories. Trajectories were calculated for each 1-min interval along the aircraft tracks and clusters of these trajectories converged reasonably well. However, relatively coarse spatial and temporal grid resolutions of the ECMWF data, together with their errors, can lead to uncertainty in the location of the center of the clusters. Secondly, mixing of air masses with ambient air during the 14-day transport can result in significant changes in chemical characteristics. Thirdly, the number of data for each air mass category is limited, especially the NMHC data. Some of the derived median values may not necessarily be representative for the September–October period.

[30] The Indonesian air constituted the dominant part (55%) of the air sampled in the upper troposphere over

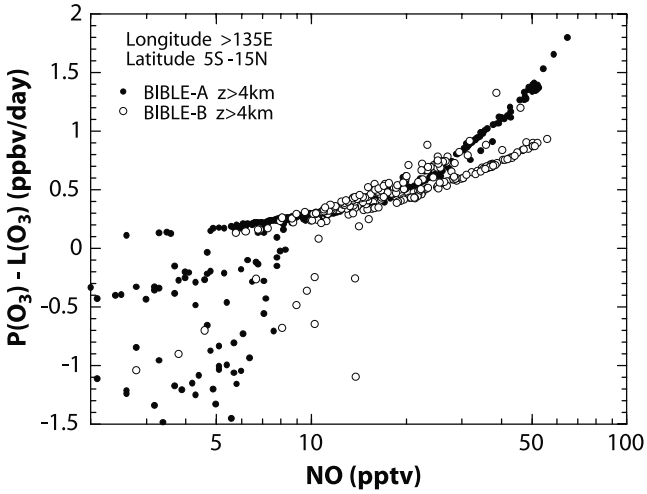

Figure 9. Net O_3 production rate in the tropical air above 4 km calculated by the AER box model.

Australia during both BIBLE A and B. In contrast, in the middle troposphere the south midlatitude air masses were sampled most frequently (31%) and Indonesian air constituted 15% of all air masses. Except for the south midlatitude air, the median values of O_3, CO, NO_y, NO, and C_2H_6 values of all the types of air masses in the upper troposphere are very similar at 44 ± 6 ppbv, 80 ± 2 ppbv, 231 ± 33 pptv, 72 ± 5 pptv, and 370 ± 35 pptv, respectively, as shown in Figure 13a and Table 2. The similarity holds also in the middle troposphere. In contrast, the median O_3, NO_y, NO, and C_2H_6 values in the south midlatitude air were considerably higher than those for the other air masses.

[31] Figure 14 shows the 10-s averaged O_3, CO, NO_y, and NO mixing ratios and their median values for south midlatitude air (red) and all air masses observed over Australia (red and black) during BIBLE A and B. The median values of these species obtained in the South Pacific south of the SPCZ at about 9°S–22°S and 160°E–140°W during PEM-T-A [*Gregory et al.*, 1999] are also shown for comparison. Many of these South Pacific air masses were transported from Africa and South America, passing over Australia, similarly to the south midlatitude air sampled during BIBLE, according to the trajectory analysis by *Board et al.* [1999]. The PEM-T-A values are similar to those in south midlatitude air in the middle troposphere, although differences are significant in the upper troposphere, reflecting the large variability. The BIBLE data, together with the PEM-T-A data characterize the chemical composition in this region impacted by biomass burning in austral spring. The values for the tropical Pacific air are also shown in Figure 14 for comparison. The O_3, CO, NO_y, and NO values over Australia were much higher than those for the tropical Pacific air.

5.2. Regional Characteristics

5.2.1. Indian Ocean and Indonesian Air

[32] The clean tropical Pacific air was carried to the Indonesian region by prevailing northwesterlies in the upper troposphere and easterlies in the lower troposphere, as seen in Figures 3 and 9. Transport of boundary layer air to the upper troposphere by convection played an important role in maintaining the levels of reactive nitrogen, CO, and NMHCs in the tropical air during its passage over Indonesia, as discussed by *Kita et al.* [2002]. The levels of CO, NO_y, C_2H_6, and C_3H_8 observed over Indonesia during BIBLE A are similar to those in Indonesian air sampled over Australia, as shown in Table 2. The C_3H_8/C_2H_6 ratios were relatively high (>0.1), most likely due to convection

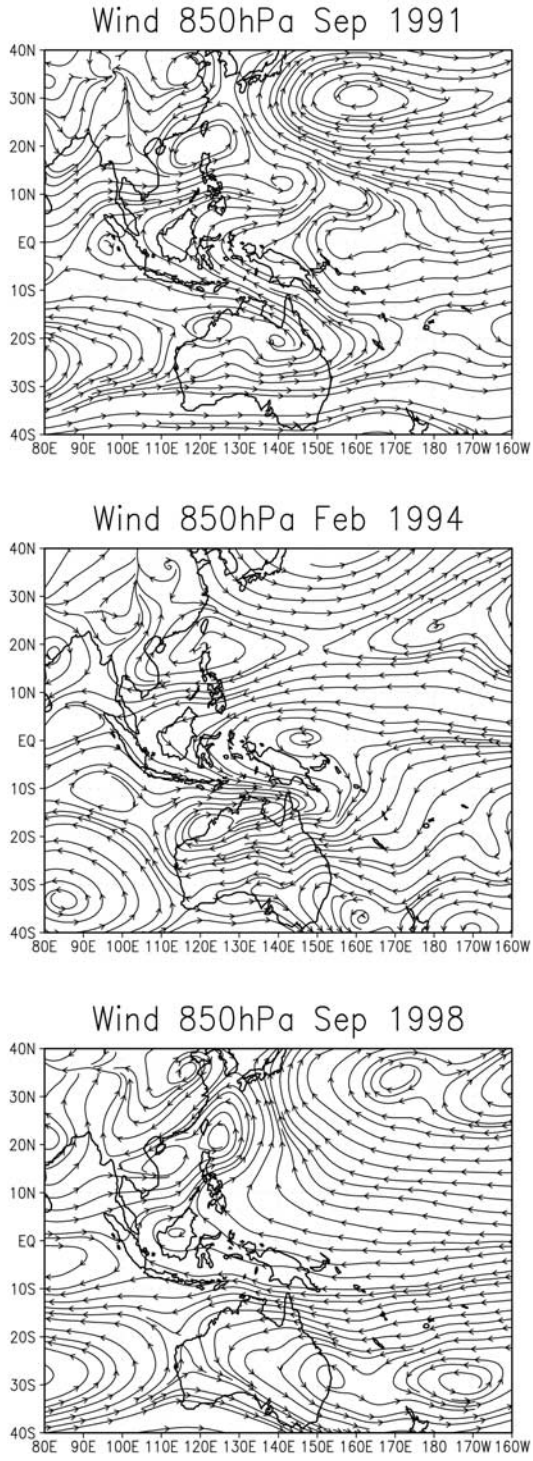

Figure 10. Average streamlines at 850 hPa in September 1991, February 1994, and September 1998.

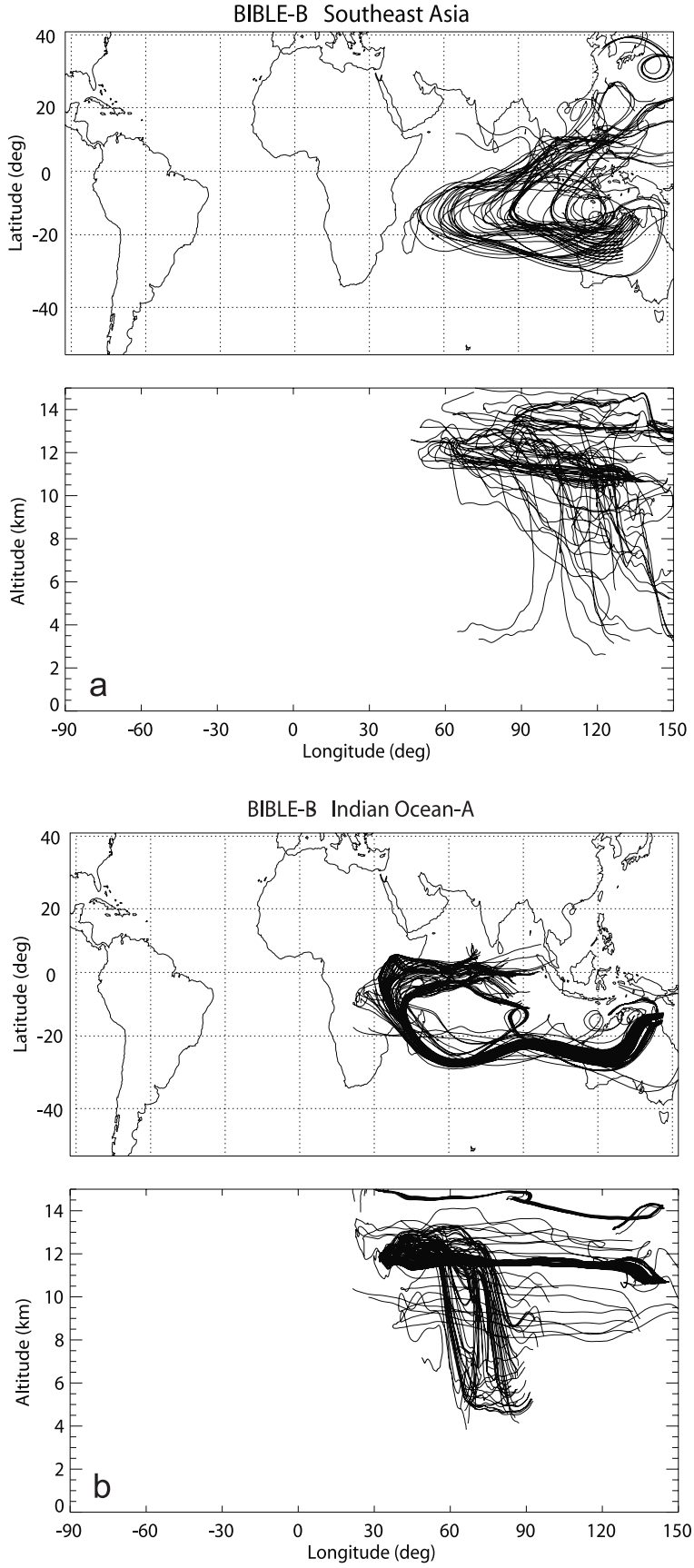

Figure 11. Fourteen-day back trajectories for air masses sampled over Australia. (a) Indonesian air plotted along the flight tack every 8 min, (b) Indian Ocean A air every 1 min, (c) Indian Ocean B air every 1 min.

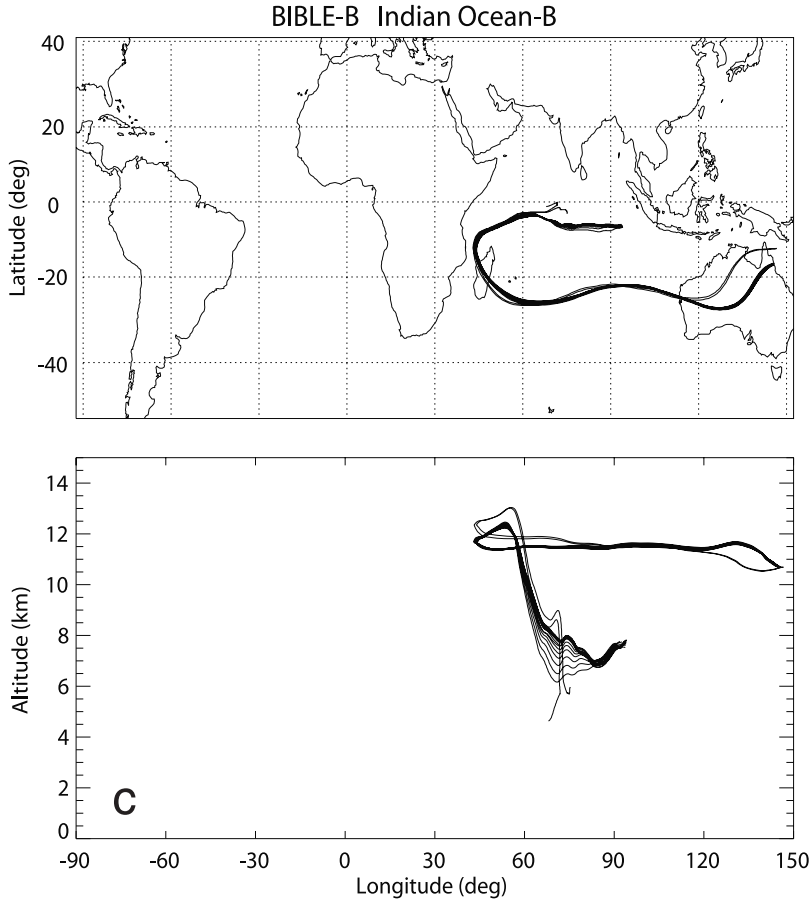

Figure 11. (continued)

near the NMHC sources over land. In addition, it was likely that lightning is the major source of NO and NO_y during BIBLE A [*Koike et al.*, 2002]. Lightning activity over Indonesia during BIBLE B was comparable to that of BIBLE A. The O_3 values increased by about 15 ppbv in Indonesian air during the week-long transport from Indonesia to Australia [*Kita et al.*, 2002] (see also Table 2). Photochemical production in the high-NO environment lead to net O_3 production rates of 2.1 ppbv/d and 1.2 ppbv/d over western Indonesia and Australia, respectively, calculated by the AER model [*Kita et al.*, 2002].

[33] Convection near the equator at 60°–90°E was responsible for the transport of Indian Ocean boundary layer air to the upper troposphere over the Indian Ocean (Figures 11b and 11c). Indian Ocean air contained aged pollutants, as evidenced by the low C_3H_8/C_2H_6 ratios of less than 0.1. It is likely that NMHCs in the boundary layer over the Indian Ocean were from anthropogenic emissions from Indonesia and northern Australia, according to the streamlines shown in Figure 6. The mixing ratios of short-lived hydrocarbons, such as C_3H_8, should decrease more rapidly than C_2H_6 during the long-range transport from these source regions before convection to the upper troposphere. In spite of the differences in origin, the NO and O_3 levels in the Indian Ocean A and B air were similar to those in the Indonesian air. At 200 hPa, the Indian Ocean air passed over Southeast Asia (Figure 6), where lightning activity was high. NO production probably elevated the NO levels in the Indian Ocean air similarly to the Indonesian air.

5.2.2. African and South Midlatitude Air

[34] The C_3H_8/C_2H_6 and n-C_4H_{10}/C_2H_6 ratios for the African upper tropospheric air were as high as the Indonesian air. It is very likely that the African air was strongly influenced by convection, as seen from the low brightness temperature of the clouds over central Africa (not shown), coinciding with the area of active convection and lightning seen from the trajectories (Figures 3 and 12). The transport of short-lived NMHCs to the upper troposphere by convection on the African continent should delay their decay, leading to high NMHC ratios similar to the Indonesian air. The average O_3, NO_y, and NO values in the upper troposphere in the African air were somewhat higher during BIBLE B than BIBLE A. The air masses during BIBLE B stayed over the Atlantic Ocean longer than during BIBLE A and might have been influenced more strongly by the African continent. However, the average O_3, NO_y, and NO values were similar to those in the Indian Ocean and Indonesian air. Causes for the similarity are not understood, considering that the African air can be more strongly impacted by extensive lightning and biomass burning over Africa, as seen in Figure 12.

[35] The high O_3, CO, NO_y, and NO values in the south midlatitude air were most pronounced in the upper troposphere, as seen in Figure 14. The south midlatitude air should have fewer chances of mixing with the clean tropical

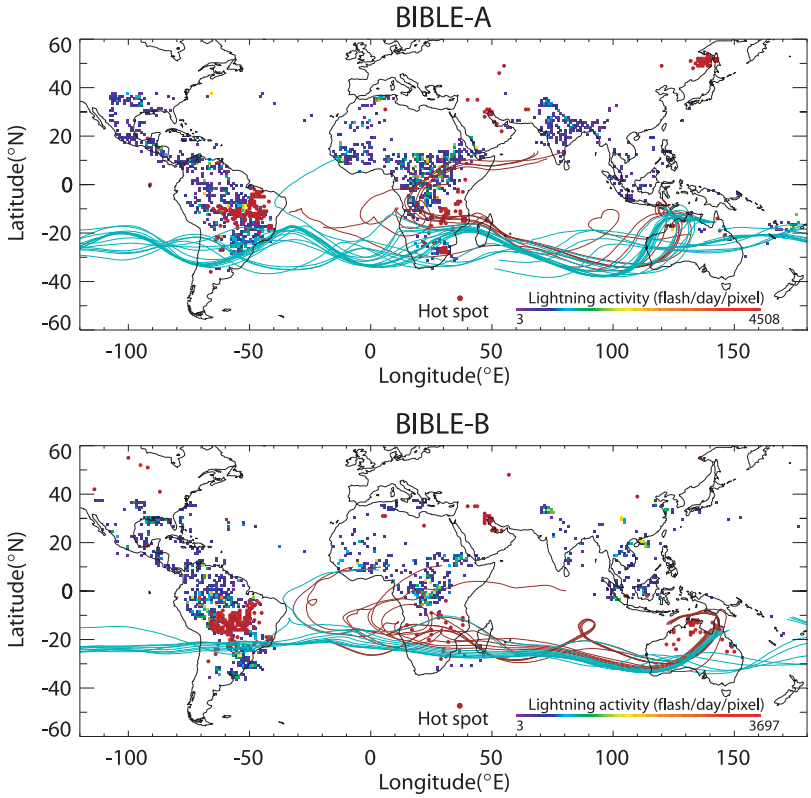

Figure 12. Fourteen-day back trajectories for African (red lines) and south midlatitude (green lines) air masses above 8 km during (top) BIBLE A and (bottom) BIBLE B. Trajectories are plotted for locations along the flight tracks every 5 min. Small squares show the locations of lightning observed by LIS. Red asterisks are intense fire counts observed by ATSR.

air than the other air masses. As shown in Figure 12, most of the south midlatitude air passed over South America and southern Africa. Emissions of the O_3 precursors from these regions should make important contributions to the precursor levels considering the magnitude of biomass burning and lightning activities on these continents. The high values of O_3, CO, NO_y, and NO, reaching 100 ppbv, 120 ppbv, 800 pptv, and 120 pptv, respectively, observed at 9–10 km during BIBLE A indicate strong effects by biomass burning. These air masses were aged, considering the low NO/NO_y and C_3H_8/C_2H_6 ratios, suggesting that they were probably not directly transported from the boundary layer over South America and southern Africa along the trajectories shown in Figure 12. Efficient accumulation of NO_y, CO, and NMHCs from these sources, without being diluted by the relatively clean tropical air, likely led to the higher values of these species in south midlatitude air.

5.3. Sources of NO_y and O_3

[36] Correlations between species emitted from biomass burning in the air observed over Australia have been used for further investigation of the sources of O_3 and NO_y. The median CH_3Cl levels were 565–595 pptv (Table 2), which are similar to those observed in the combustion plumes during PEM-T-A [*Talbot et al.*, 2000]. Low levels of C_2Cl_4 (1.1 pptv) and its poor correlation with CO exclude significant effects from industrial activities. Correlations between CO, NO_y, and O_3 for south midlatitude air and all the air types observed over Australia at 4–8 km and above 8 km are shown in Figure 15, together with the correlation coefficients (r^2). NO_y and O_3 were well correlated with CO for CO values lower than 90 ppbv in the middle troposphere. Many of the data with CO higher than 90 ppbv in the middle troposphere were obtained at 4–5 km (Figure 14). This means that O_3 correlated well with CO above 5 km during both BIBLE A and B. During PEM-T-A, O_3 was also positively correlated with CO ($r^2 = 0.49$) above 4 km over the South Pacific [*Blake et al.*, 1999]. The NO_y-CO correlation was poorer in the upper troposphere, suggesting combinations of different sources of NO_y, depending on air masses. In fact, lightning has been identified as a primary source of NO_y over Indonesia [*Koike et al.*, 2002].

5.3.1. Biomass Burning Source of NO_y

[37] Variability in CO ranging from 60 to 140 ppbv must have been caused mostly by biomass burning, because it is the dominant anthropogenic source of CO in the Southern Hemisphere [*Wang et al.*, 1998]. Although CO production by CH_4 and NMHC oxidation constitutes 60% of the total CO production in the Southern Hemisphere, it should not cause large variability such as that observed during BIBLE. In fact, the background CO mixing ratios between 2–12 km ranged between 50 and 70 ppbv from the equator to 50°S at 100°–160°W with no strong systematic latitudinal dependence during PEM-T-A, except in biomass burning plumes encountered mostly at 160°W–170°E [*Blake et al*, 1999]. NO_y is produced simultaneously with CO in the boundary

Table 2. Median Values and Number of Data Points for Each Type of Air Mass Sampled Over Australia and Indonesia[a]

			Over Australia				
	South Midlatitude	Africa	Indian Ocean A	Indian Ocean B	Indonesia	All Air Masses	Over Indonesia BIBLE A
				O_3(ppbv)			
>8 km	84 (94, 77)	51 (35, 55)	41 (33, 45)	44 (99, 44)	38 (34, 39)	40 (36, 41)	23
4–8 km	62 (73, 61)	42 (72, 36)	60 (-, 60)	34 (29, 34)	38 (37, 39)	47 (40, 48)	20
				CO (ppbv)			
>8 km	84 (104, 77)	80 (81, 80)	79 (84, 79)	77 (96, 77)	82 (81, 82)	81 (83, 81)	81
4–8 km	80 (107, 80)	74 (112, 74)	80 (-, 80)	74 (75, 74)	76 (80, 76)	78 (80, 78)	73
				NO_y(pptv)			
>8 km	434 (615, 310)	244 (193, 263)	216 (181, 228)	265 (641, 265)	198 (153, 220)	221 (192, 234)	164
4–8 km	313 (353, 312)	195 (403, 190)	263 (-, 263)	162 (89, 178)	167 (146, 168)	227 (160, 231)	84
				NO (pptv)			
>8 km	108 (114, 93)	82 (67, 99)	69 (62, 70)	68 (69, 67)	67 (50, 70)	71 (68, 73)	52
4–8 km	24 (25, 23)	15 (23, 15)	27 (-, 27)	18 (12, 19)	24 (22, 25)	21 (20, 21)	10
				C_2H_6(pptv)			
>8 km	523 (554, 400)	387 (389, 387)	335 (352, 335)	395 (453, 395)	364 (364, 364)	377 (384, 372)	361
4–8 km	397 (320, 398)	305 (692, 302)	373 (-, 373)	317 (332, 307)	324 (352, 322)	348 (332, 354)	330
				C_3H_8(pptv)			
>8 km	39 (37, 39)	53 (75, 51)	30 (82, 28)	32 (49, 31)	47 (60, 41)	43 (56, 41)	48
4–8 km	33 (20, 34)	22 (43, 21)	26 (-, 26)	26 (26, 26)	29 (39, 29)	26 (28, 26)	24
				CH_3Cl (pptv)			
>8 km	567 (559, 606)	572 (557, 602)	580 (571, 589)	593 (553, 599)	582 (571, 593)	582 (565, 595)	577
4–8 km	593 (572, 595)	580 (576, 580)	591 (-, 591)	585 (569, 589)	583 (555, 587)	588 (568, 590)	580
				Number of Data Points for O_3, CO, NO_y, and NO			
>8 km	664 (420, 244)	467 (220, 247)	518 (115, 403)	414 (42, 372)	2484 (760, 1724)	4547 (1557, 2990)	4124
4–8 km	555 (29, 526)	255 (30, 225)	355 (-, 355)	352 (79, 273)	266 (53, 213)	1783 (191, 1592)	1729
				Number of Data Points for C_2H_6, C_3H_8, and CH_3Cl			
>8 km	17 (11, 6)	17 (9, 8)	15 (4, 11)	11 (2, 9)	76 (25, 51)	136 (51, 85)	172
4–8 km	33 (1, 32)	21 (2, 19)	18 (-, 18)	16 (6, 10)	19 (2, 17)	107 (11, 96)	102

[a]For species concentrations, the three numbers for the entry are given in the format X (A, B) where X is the median value for all the BIBLE A and BIBLE B data sets, A is the median value for BIBLE A, and B is the median values for BIBLE B. The number of data points is given in the last four rows with the same format except the integer corresponds to the number of data points. The column labeled "all air masses" represents all data taken over Australia and corresponds to the aggregates of data listed in the five columns to its left.

layer by combustion. Thus, the observed tight correlation above 5 km is consistent with this source.

5.3.2. Stratospheric Intrusion as a Source of Ozone and NO_y

[38] NO_y and O_3 are also transported from the lowermost stratosphere, where NO_y and O_3 are negatively correlated with CO [*Singh et al.*, 1997]. In some air masses CO was as low as 65 ppbv, while O_3 was as high as 80 ppbv at 13 km, as seen in the O_3-CO correlation, suggesting some stratospheric influence. The NO_y and O_3 mixing ratios should increase with latitude if stratospheric injection were the dominant NO_y source in the troposphere, because stratosphere-troposphere exchange is most efficient at midlatitudes [*Holton et al.*, 1995]. NO_y and O_3 can be positively correlated with CO in the stratospheric air after mixing with tropospheric air only if the background CO mixing ratio increases with latitude, which was not the case, as described above. Therefore, the overall positive correlations of NO_y and O_3 with CO at 4–13 km indicate that influx from the stratosphere was not generally a dominant source of NO_y and O_3. Impact of biomass burning on NO_y and O_3 is considered to be strong in south midlatitude air, where the CO values sometimes exceeded 100 ppbv, as discussed in section 5.2.2.

5.3.3. Lightning as a Source of NO_y

[39] During upward transport by active convection, lightning can add a significant amount of NO to the biomass burning plumes already rich in NO_y and CO. Lightning was observed in the locations adjacent to the regions of active biomass burning over South America and south Africa, as seen in Figure 12. This makes it very difficult to separate contributions from the two different sources in these regions. Because mixing with ambient air and chemical processing of combustion plumes during transport continues to change the NO_y-CO correlation, it is even more difficult to separate the contribution of lightning from the correlation observed over Australia. An independent estimate by the Geophysical Fluid Dynamics Laboratory global chemical transport model shows that lightning is estimated to make the largest contribution to the NO_x abundance in the free troposphere at latitudes north of 30°–40°S over Australia, while NO_x from biomass burning is estimated to be more important at higher latitudes, between June and August [*Levy et al.*, 1999].

5.3.4. Photochemical Production of Ozone

[40] Ozone was correlated with NO_y more tightly than it was with CO. This is expected from the strong dependence of the net O_3 production rate on the NO value (Figure 9).

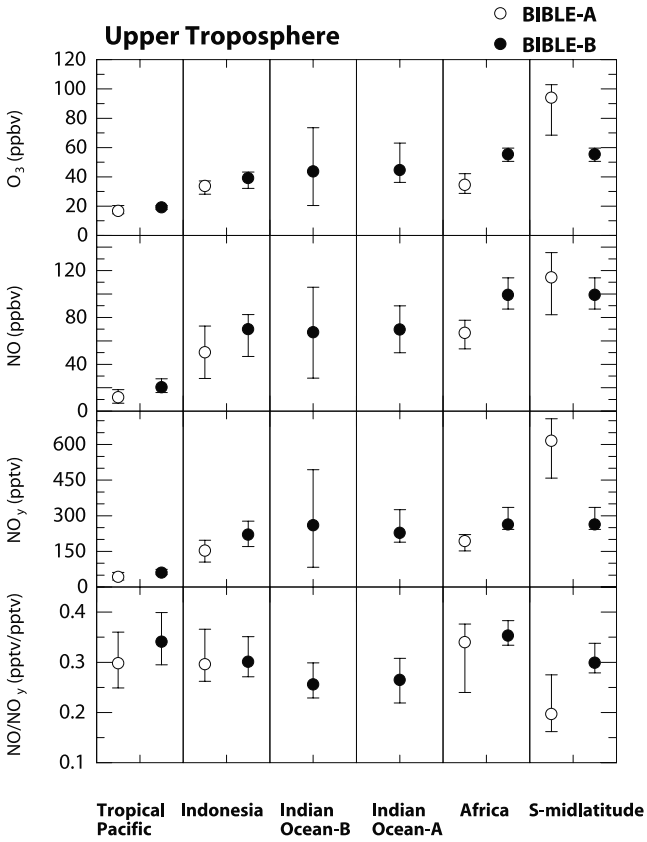

Figure 13a. Median values of O_3, NO, NO_y, and NO/NO_y ratios obtained in the upper troposphere in tropical Pacific, Indonesian, Indian Ocean A and B, African, and south midlatitude air during BIBLE A (open circles) and BIBLE B (solid circles).

Net O_3 production rates in the upper troposphere over Australia were 1–1.5 ppbv/d at NO mixing ratios of 60–120 pptv. The O_3 production rates were lower in the middle troposphere because the NO levels were lower. The O_3 production during the transport should tighten the NO_y-O_3 correlation. The slope of the NO_y-O_3 correlation has been found to increase from 0.014 to 0.10 ppbv/pptv during the transport from Indonesia to northern Australia in about 7 days [*Kita et al.*, 2002]. This data set constitutes a part of the NO_y-O_3 correlation in Figure 15. This phenomenon also occurred in air masses in the upper troposphere over the tropical Pacific when there was significant O_3 production in a relatively high-NO environment as shown in Figure 8. The average NO_y-O_3 correlation obtained in the lowermost stratospheric air at northern midlatitudes [*Koike et al.*, 1997] was extrapolated to lower NO_y and O_3 values. These values are shown in Figure 15 for comparison. The NO_y-O_3 correlation observed over Australia was similar to that for the extrapolated lowermost stratospheric air, despite the significant influence of biomass burning on NO_y indicated from the NO_y-CO correlation, as discussed above. The NO_x-catalyzed O_3 production and relatively small loss of NO_y in the upper troposphere, together with mixing/dilution, probably led to a steady state characterized by the observed NO_y-O_3 correlation.

6. Summary and Conclusions

[41] The mixing ratios of O_3, CO, NO_y, NO, and NMHCs over the western Pacific Ocean in August–October 1998 and 1999 showed large latitudinal variations from northern midlatitudes to the equatorial region, with the lowest values at 15°N–5°S throughout all altitudes. The range of their median mixing ratios at different altitudes were 5–20 ppbv, 60–75 ppbv, 20–100 pptv, and 5–40 pptv, respectively. A trajectory analysis demonstrates that the tropical Pacific air was transported from the boundary layer at 15°N–5°S east of the sampling locations through extensive convection in the ITCZ, indicating that the tropical air was nearly completely isolated from midlatitude air. Similar low values were observed in the upper troposphere over the same region during PEM-W-A in September–October and in convective air masses during PEM-W-B in February. However, the PEM-W-A values were somewhat higher than those during BIBLE due to prevailing westerly winds in the lower troposphere, transporting air impacted by Southeast Asia to the tropical Pacific. These results indicate the influence of ENSO on the chemical composition of the tropical Pacific air through the changes in the lower tropospheric winds. NO and NO_y values reaching 300–1000 pptv were often observed at 10–12 km, due to the NO production by lightning near New Guinea during BIBLE A and B and PEM-W-B, as expected from the frequent lightning flashes observed by LIS and high convective activity in October–March.

[42] The air impacted by biomass burning that occurred in northern Australia was mostly confined to the boundary layer due to strong subsidence. Free tropospheric air masses sampled over Australia at 10°–28°S were classified according to their origins determined using 14-day back trajectories: Indonesia, Indian Ocean A, Indian Ocean B, Africa, and south midlatitude. Indonesian air constituted 55% of the all air masses sampled in the upper troposphere. The median values of O_3, CO, NO_y, NO, and C_2H_6 values above 8 km in all the types of air except for the south midlatitude air, were similar at about 44 ± 6 ppbv, 80 ± 2 ppbv, 230 ± 30 pptv, 72 ± 5pptv, and 370 ± 35 pptv, respectively. These concentrations are much higher than those observed in the tropical Pacific air.

[43] The relatively high C_3H_8/C_2H_6 and n-C_4H_{10}/C_2H_6 ratios in Indonesian air indicate rapid transport of the continental boundary layer air to the upper troposphere, where the lifetimes of the short-lived NMHCs are longer. Lightning likely increased the levels of NO and NO_y in the Indonesian air, considering that the NO levels over Indonesia were strongly impacted by lightning during BIBLE A [*Koike et al.*, 2002]. Photochemical production in the high-NO environment elevated the O_3 values by 15 ppbv during transport from Indonesia to Australia [*Kita et al.*, 2002]. The NMHC ratios were lower in the Indian Ocean air that was transported over long distances from continental sources before being transported to the upper troposphere. The NO levels in the Indian Ocean air were probably influenced by lightning over Southeast Asia, as in the Indonesian air.

[44] African air in the upper troposphere was strongly influenced by convection and lightning over central Africa, consistent with the high NMHC ratios. However, the median O_3, NO_y, and NO values were not especially high

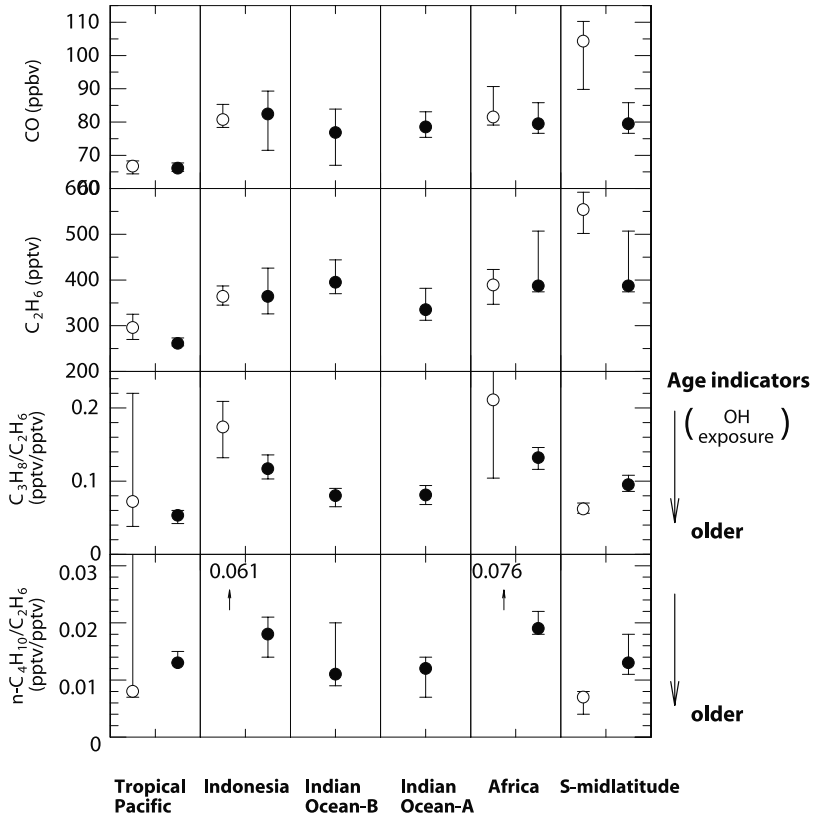

Figure 13b. Same as Figure 13a but for CO, C_2H_6, C_3H_8/C_2H_6, and n-C_4H_{10}/C_2H_6.

when compared with those in the Indian Ocean and Indonesian air. The O_3, NO, NO_y, CO, and C_2H_6 values were highest in the south midlatitude air masses at 5–13 km. The upper tropospheric values were particularly high. The PEM-T-A values obtained in the South Pacific south of the SPCZ are similar to those in south midlatitude air in the middle troposphere, although differences are significant in the upper troposphere, reflecting the large variability. The south midlatitude air masses sampled during BIBLE A were significantly aged, suggesting that they had not recently been impacted by biomass burning over South America and Africa. Efficient accumulation of NO_y, CO, O_3, and NMHCs from these sources, without significant dilution by the relatively clean tropical air, likely augmented the values of these species in the south midlatitude air.

[45] The enhancements in CO above the background levels in the free troposphere over Australia was due mainly to the emissions from biomass burning, considering that it is the dominant anthropogenic source of CO in the Southern Hemisphere. The positive and reasonably tight correlations of NO_y and O_3 with CO indicate that NO_y and O_3 were impacted by biomass burning. The biomass burning signature was strong in south midlatitude air, where the CO values sometimes exceeded 100 ppbv.

[46] Although lightning was likely an important source of NO in Indonesian air, separating the effects of lightning and biomass burning on the observed NO and NO_y is difficult for African and south midlatitude air because biomass burning occurred in the areas adjacent to the intensive lightning regions over Africa and South America.

[47] O_3 was correlated with NO_y more tightly than with CO, mainly due to the strong dependence of the net O_3 production rate on the NO abundances, irrespective of the NO and NO_y sources (biomass burning or lightning). The NO_x-catalyzed O_3 production and relatively small loss of NO_y in the upper troposphere, together with mixing/dilution, probably led to a steady state characterized by the observed NO_y-O_3 correlation.

[48] **Acknowledgments.** This work was supported by the BIBLE program at NASDA EORC. Construction of the CO instrument used for BIBLE B was supported by D.D. Parrish, J. Holloway, and F.C. Fehsenfeld of NOAA. The meteorological data were supplied by the European Centre for Medium-Range Weather Forecasts (ECMWF). Partial funding by the Japanese MEXT is gratefully acknowledged. Assistance in the data processing by D. Akutagawa is greatly appreciated.

References

Blake, D. R., T. Y. Chen, T. W. Smith Jr., C. J.-L. Wang, O. W. Wingenter, N. J. Blake, F. S. Rowland, and E. W. Mayer, Three-dimensional distribution of NMHCs and halocarbons over the northwestern Pacific during the 1991 Pacific exploratory Mission (PEM WEST-A), *J. Geophys. Res.*, *101*, 1763–1778, 1996.

Blake, N. J., et al., Influence of Southern Hemispheric biomass burning on midtropospheric distributions of nonmethane hydrocarbons and selected halocarbons over the remote South Pacific, *J. Geophys. Res.*, *104*, 16,213–16,232, 1999.

Board, A. S., et al., Chemical characteristics of air from differing source regions during the Pacific Exploratory Mission-Tropics A (PEM-Tropics A), *J. Geophys. Res.*, *104*, 16,181–16,196, 1999.

Emmons, L. K., et al., Climatologies of NO_x and NO_y: A comparison of data and models, *Atmos. Environ*, *31*, 1851–1904, 1997.

Emmons, L. K., et al., Data composites of airborne observations of tropospheric ozone and its precursors, *J. Geophys. Res.*, *105*, 20,497–20,538, 2000.

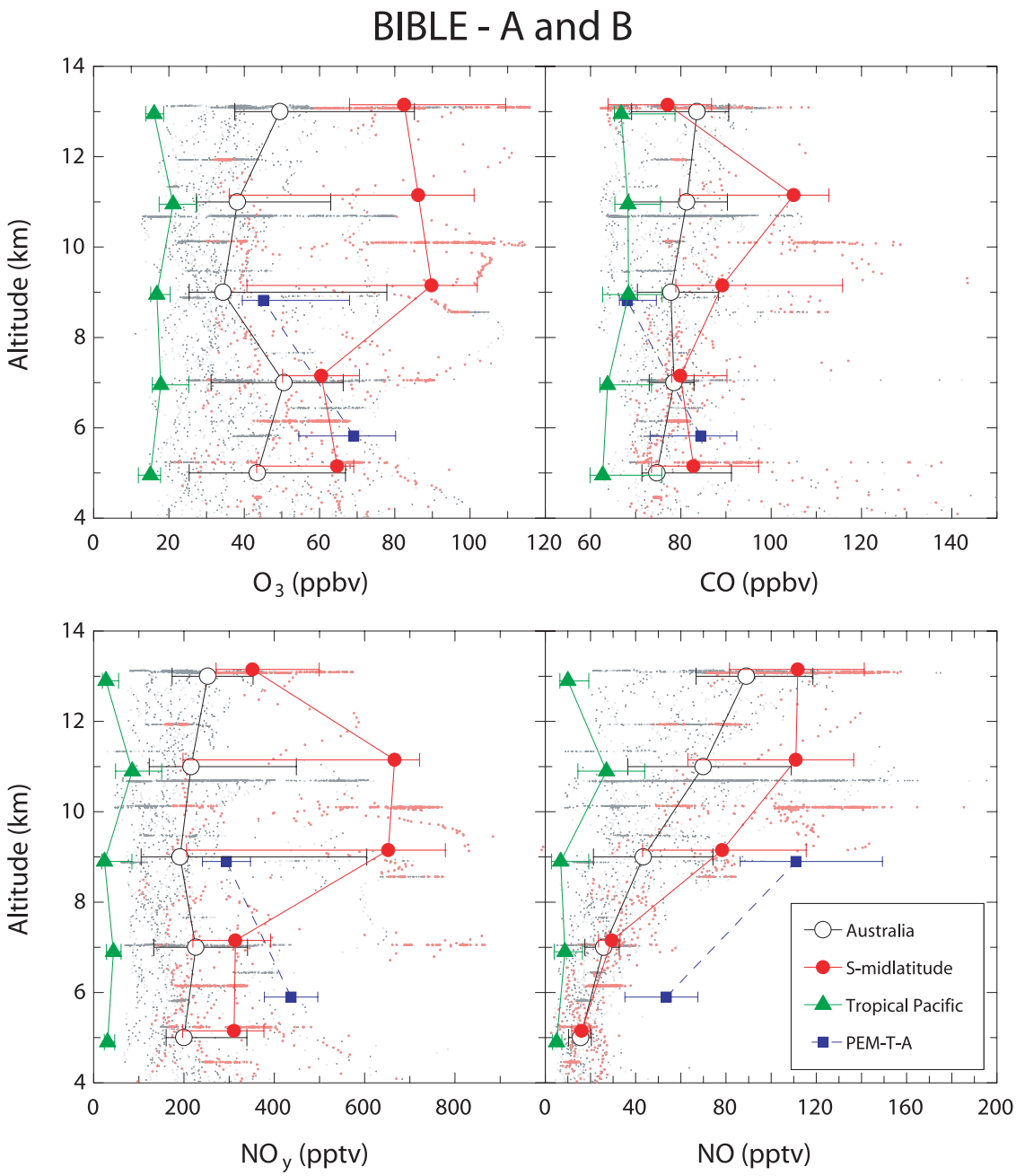

Figure 14. Profiles of 10-s averaged data of O_3, CO, NO_y, and NO obtained in south midlatitude air (small red points) and all air masses sampled over Australia (small black and red points) during BIBLE A and B, together with the median values (large circles with bars). The data for the tropical Pacific Ocean (green) and those observed in the South Pacific south of SPCZ during PEM-T-A by *Gregory et al.* [1999] (blue squares) are also shown for comparison. The bars represent the central 67% of the range.

Fenn, M. A., et al., Ozone and aerosol distributions and air mass characteristics over the South Pacific during the burning season, *J. Geophys. Res.*, *104*, 16,197–16,212, 1999.

Fuelberg, H. E., et al., A meteorological overview of the Pacific Exploratory Mission (PEM) Tropics period, *J. Geophys. Res.*, *104*, 5585–5622, 1999.

Gregory, G. L., A. S. Bachmeier, D. R. Blake, B. G. Heikes, D. C. Thornton, J. D. Bradshaw, and Y. Kondo, Chemical signatures of aged Pacific marine air: Mixed layer and free troposphere as measured during PEM West-A, *J. Geophys. Res.*, *101*, 1727–1742, 1996.

Gregory, G. L., J. T. Merrill, M. C. Shipham, D. R. Blake, G. W. Sachse, and H. B. Singh, Chemical characteristics of tropospheric air over the Pacific Ocean as measured during PEM-West B: Relationship to Asian outflow and trajectory history, *J. Geophys. Res.*, *102*, 28,275–28,285, 1997.

Gregory, G. L., et al., Chemical characteristics of Pacific tropospheric air in the region of the Intertropical Convergence Zone and South Pacific Convergence Zone, *J. Geophys. Res.*, *104*, 5677–5696, 1999.

Holton, J. R., P. H. Haynes, M. E. McIntyre, A. R. Douglass, R. B. Rood, and L. Pfister, Stratosphere-troposphere exchange, *Rev. Geophys*, *33*, 403–439, 1995.

Kawakami, S., et al., Impact of lightning and convection on reactive nitrogen in the tropical free troposphere, *J. Geophys. Res.*, *102*, 28,367–28,384, 1997.

Kita, K., et al., Photochemical production of ozone in the upper troposphere in association with cumulus convection over Indonesia, *J. Geophys. Res.*, doi:10.1029/2001JD000844, in press, 2002.

Klonecki, A. A., and H. Levy II, Tropospheric chemical ozone tendencies in CO-CH_4-NO_y-H_2O system: Their sensitivity to variations in environ-

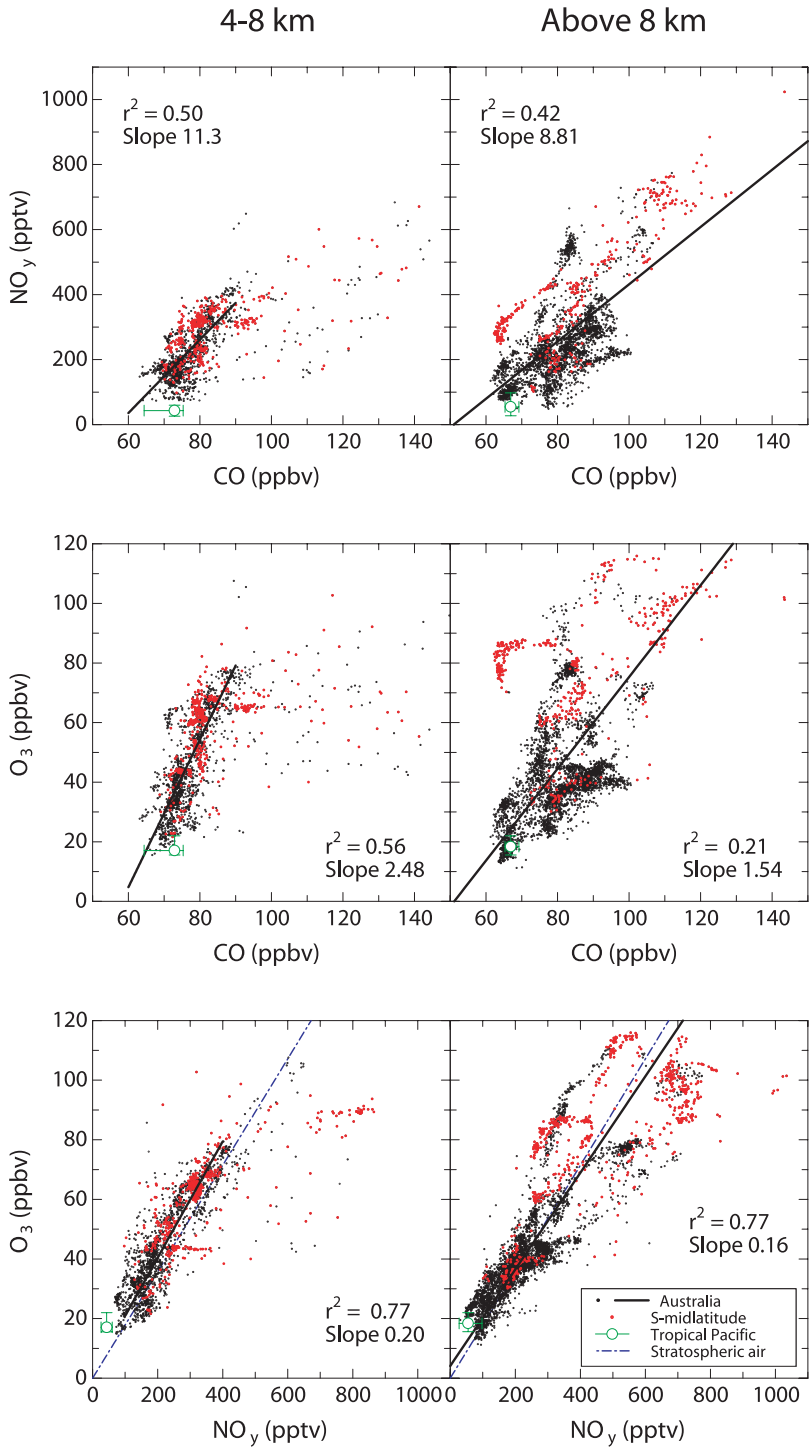

Figure 15. NO_y-CO, O_3-CO, and O_3-NO_y correlations obtained at 4–8 km and 8–13 km in south midlatitude air (red points) and all air masses sampled over Australia (black and red points) during BIBLE A and B. The data for the tropical Pacific Ocean (green) are also shown for comparison. The black straight lines are least squares fits to all the data obtained over Australia. At 4–8 km, data with CO and NO_y mixing ratios lower than 90 ppbv and 400 pptv were used for this fit. Blue dashed lines in the O_3-NO_y correlations represent the relationship for lowermost stratosphere at northern midlatitudes extended to lower NO_y and O_3 values.

mental parameters and their application to a global chemistry transport model study, *J. Geophys. Res.*, *102*, 21,221–21,237, 1997.

Ko, M., W. Hu, J. Rodriguez, Y. Kondo, M. Koike, K. Kita, S. Kawakami, D. Blake, S. Liu, and T. Ogawa, Photochemical ozone budget during the BIBLE A and B campaigns, *J. Geophys. Res.*, doi:10.1029/2001JD000800, in press, 2002.

Koike, M., Y. Kondo, S. Kawakami, H. Nakajima, G. L. Gregory, G. W. Sachse, H. B. Singh, E. V. Browell, J. T. Merrill, and R. E. Newell, Reactive nitrogen and its correlation with O_3 and CO over the Pacific in winter and early spring, *J. Geophys. Res.*, *102*, 28,385–28,404, 1997.

Koike, M., et al., Impact of aircraft emissions on reactive nitrogen over the North Atlantic Flight Corridor region, *J. Geophys. Res.*, *105*, 3665–3677, 2000.

Koike, M., Reactive nitrogen over the tropical western Pacific: Influence from lightning and biomass burning during BIBLE A, *J. Geophys. Res*, doi:10.1029/2001JD000823, in press, 2002.

Kondo, Y., T. Kitada, M. Koike, S. Kawakami, and Y. Makino, Nitric oxide and ozone in the free troposphere over the western Pacific Ocean, *J. Geophys. Res.*, *98*, 28,527–28,535, 1993.

Kondo, Y., H. Ziereis, M. Koike, S. Kawakami, G. L. Gregory, G. W. Sachse, H. B. Singh, D. D. Davis, and J. T. Merrill, Reactive nitrogen over the Pacific ocean during PEM-West A, *J. Geophys. Res.*, *101*, 1809–1828, 1996.

Kondo, Y., S. Kawakami, M. Koike, D. W. Fahey, H. Nakajima, Y. Zhao, N. Toriyama, M. Kanada, G. W. Sachse, and G. L. Gregory, The performance of an aircraft instrument for the measurement of NO_y, *J. Geophys. Res.*, *102*, 28,663–28,671, 1997a.

Kondo, Y., M. Koike, S. Kawakami, H. B. Singh, R. Talbot, H. Nakajima, G. L. Gregory, D. R. Blake, G. W. Sachse, and J. T. Merrill, Profiles and partitioning of reactive nitrogen over the Pacific Ocean in winter and early spring, *J. Geophys. Res.*, *102*, 28,405–28,424, 1997b.

Levy, H., II, W. J. Moxim, K. A. Klonecki, and P. S. Kashibhatla, Simulated tropospheric NO_x: Its evaluation, global distribution and individual source contributions, *J. Geophys. Res.*, 26,279–26,306, 1999.

Matsuzono, T., T. Sano, and T. Ogawa, Development of the trajectory analysis model (EORC/TAM), *EORC Bull. Tech. Rep. 1*, edited by T. Igarashi, pp. 55–68, Natl. Space Dev. Agency of Jpn., Tokyo, 1998.

Mauzerall, D. L., et al., Photochemistry in biomass burning plumes and implications for tropospheric ozone over the tropical South Atlantic, *J. Geophys. Res.*, *103*, 8401–8423, 1998.

McKeen, S. A., and S. C. Liu, Hydrocarbon ratios and photochemical history of air masses, *Geophys. Res. Lett.*, *20*, 2363–2366, 1993.

McKeen, S. A., S. C. Liu, E.-Y. Hsie, X. Lin, J. D. Bradshaw, S. Smyth, G. L. Gregory, and D. R. Blake, Hydrocarbon ratios during PEM-West A: A model perspective, *J. Geophys. Res.*, *101*, 2087–2109, 1996.

Nesbitt, S. W., R. Zhang, and R. E. Orville, Seasonal and global NO_x production by lightning estimated from Optical Transient Detector (OTD), *Tellus, Ser. B*, *52*, 1206–1215, 2000.

Nishi, N., Meteorological fields which affect the transport and chemical processes during the Biomass Burning and Lightning Experiment Phase-A and B (BIBLE-A, B), *NASDA EORC Tech. Rep. 7*, pp. 36–52, Natl. Space Dev. Agency of Jpn., Tokyo, 2001.

Russell-Smith, J., A. C. Edwards, and G. D. Cook, Reliability of biomass burning estimates from savanna fires: Biomass burning in northern Australia during the 1999 Biomass Burning and Lightning Experiment B field campaign, *J. Geophys. Res*, doi:10.1029/2001JD000787, in press, 2002.

Shirai, T., et al., Emission estimates of selected volatile organic compounds from tropical savanna burning in northern Australia, *J. Geophys. Res*, doi:10.1029/2001JD000841, in press, 2002.

Singh, H. B., Y. Chen, G. L. Gregory, G. W. Sachse, R. Talbot, D. R. Blake, Y. Kondo, J. D. Bradshaw, B. Heikes, and D. Thornton, Trace chemical measurements from the northern mid-latitude lowermost stratosphere in early spring: Distributions, correlations, and fate, *Geophys. Res. Lett*, *24*, 127–130, 1997.

Singh, H. B., Latitudinal distribution of reactive nitrogen in the free troposphere over the Pacific Ocean in late winter/early spring, *J. Geophys. Res.*, *103*, 28,237–28,246, 1998.

Takegawa, N., et al., Airborne vacuum ultraviolet resonance fluorescence instrument for in situ measurement of CO, *J. Geophys. Res.*, *106*, 24,237–24,244, 2001.

Talbot, R. W., et al., Tropospheric reactive odd nitrogen over the South Pacific in austral spring, *J. Geophys. Res.*, *105*, 6681–6694, 2000.

Wang, Y., D. J. Jacob, and J. A. Logan, Global simulation of tropospheric O_3-NO_x-hydrocarbon chemistry, 2, Model evaluation and global ozone budget, *J. Geophys. Res.*, *103*, 10,727–10,755, 1998.

D. Blake, Department of Chemistry, University of California, Irvine, Irvine, CA 92697-2025, USA. (drblake@uci.edu)

Y. Higashi, H. Ikeda, K. Kita, Y. Kondo, Y. Miyazaki, and N. Takegawa, Research Center for Advanced Science and Technology, University of Tokyo, 4-6-1 Komaba, Meguro, Tokyo 153-8904, Japan. (yoko@aos.eps.s.u-tokyo.ac.jp; hibiki@atmos.rcast.u-tokyo.ac.jp; kita@atmos.rcast.u-tokyo.ac.jp; kondo@atmos.rcast.u-tokyo.ac.jp; yuzom@aos.eps.s.u-tokyo.ac.jp; takegawa@atmos.rcast.u-tokyo.ac.jp)

H. Irie, Solar-Terrestrial Environment Laboratory, Nagoya University, 3-13 Honohara, 442-8507,Toyokawa, Japan. (irie@atmos.rcast.u-tokyo.ac.jp)

S. Kawakami and T. Ogawa, National Space Development Agency of Japan, Earth Observation Research Center, Tokyo, Japan. (kawakami@eorc.nasda.go.jp; t_ogawa@eorc.nasda.go.jp)

M. Ko, Atmospheric and Environmental Research, Inc., 131 Hartwell Avenue, Lexington, MA 02421-3126, USA. (mko@aer.com)

M. Koike, Department of Earth and Planetary Physics, Graduate School of Science, University of Tokyo, 7-3-1 Hongo, Bunkyo-ku, Tokyo 113-0033, Japan. (koike@eps.s.u-tokyo.ac.jp)

N. Nishi, Department of Earth and Planetary Science, Graduate School of Science, Kyoto University, Kitashirakawa-Oiwakecho, Sakyo-ku, Kyoto 606-8502, Japan. (nishi@kugi.kyoto-u.ac.jp)

B. Liley, National Institute of Water and Atmospheric Research, Private Bag 50061, Omakau, Lauder 9182, New Zealand. (b.liley@niwa.cri.nz)

S. C. Liu, Institute of Earth Sciences, Academia Sinica, P.O. Box 1-55, Nankang, Taipei 11529, Taiwan. (shawliu@earth.sinica.edu.tw)

Y. Zhao, Department of Mechanical and Aeronautical Engineering, University of California, Davis, One Shields Avenue, Davis, CA 95616, USA. (yzhao@mae.ucdavis.edu)